A Section 508–conformant HTML version of this article is available at https://doi.org/10.1289/EHP12034.

Effects of Cyanobacterial Harmful Algal Bloom Toxin Microcystin-LR on Gonadotropin-Dependent Ovarian Follicle Maturation and Ovulation in Mice

Yingzheng Wang,[1,2,3,4,5] Pawat Pattarawat,[1,2] Jiyang Zhang,[1,2] Eunchong Kim,[1,2] Delong Zhang,[1,2] Mingzhu Fang,[6] Elizabeth A. Jannaman,[7] Ye Yuan,[7] Saurabh Chatterjee,[8,9] Ji-Yong Julie Kim,[10] Geoffrey I. Scott,[3,4] Qiang Zhang,[11] and Shuo Xiao[1,2,4,5]

[1]Department of Pharmacology and Toxicology, Ernest Mario School of Pharmacy, Rutgers University, Piscataway, New Jersey, USA
[2]Environmental and Occupational Health Sciences Institute, Rutgers University, Piscataway, New Jersey, USA
[3]Department of Environmental Health Sciences, Arnold School of Public Health, University of South Carolina, Columbia, South Carolina, USA
[4]National Institute of Environmental Health Sciences Center for Oceans and Human Health and Climate Change Interactions at the University of South Carolina, Columbia, South Carolina, USA
[5]Center for Environmental Exposures and Disease, Rutgers University, Piscataway, New Jersey, USA
[6]New Jersey Department of Environmental Protection, Trenton, New Jersey, USA
[7]Colorado Center for Reproductive Medicine, Lone Tree, Colorado, USA
[8]Department of Environmental and Occupational Health, University of California, Irvine, Irvine, California, USA
[9]Division of Infectious Disease, Department of Medicine, University of California, Irvine, Irvine, California, USA
[10]Department of Obstetrics and Gynecology, Feinberg School of Medicine, Northwestern University, Chicago, Illinois, USA
[11]Gangarosa Department of Environmental Health, Rollins School of Public Health, Emory University, Atlanta, Georgia, USA

Background: Cyanobacterial harmful algal blooms (CyanoHABs) originate from the excessive growth or bloom of cyanobacteria often referred to as blue-green algae. They have been on the rise globally in both marine and freshwaters in recently years with increasing frequency and severity owing to the rising temperature associated with climate change and increasing anthropogenic eutrophication from agricultural runoff and urbanization. Humans are at a great risk of exposure to toxins released from CyanoHABs through drinking water, food, and recreational activities, making CyanoHAB toxins a new class of contaminants of emerging concern.

Objectives: We investigated the toxic effects and mechanisms of microcystin-LR (MC-LR), the most prevalent CyanoHAB toxin, on the ovary and associated reproductive functions.

Methods: Mouse models with either chronic daily oral or acute intraperitoneal exposure, an engineered three-dimensional ovarian follicle culture system, and human primary ovarian granulosa cells were tested with MC-LR of various dose levels. Single-follicle RNA sequencing, reverse transcription–quantitative polymerase chain reaction, enzyme-linked immunosorbent assay, western blotting, immunohistochemistry (IHC), and benchmark dose modeling were used to examine the effects of MC-LR on follicle maturation, hormone secretion, ovulation, and luteinization.

Results: Mice exposed long term to low-dose MC-LR did not exhibit any differences in the kinetics of folliculogenesis, but they had significantly fewer corpora lutea compared with control mice. Superovulation models further showed that mice exposed to MC-LR during the follicle maturation window had significantly fewer ovulated oocytes. IHC results revealed ovarian distribution of MC-LR, and mice exposed to MC-LR had significantly lower expression of key follicle maturation mediators. Mechanistically, in both murine and human granulosa cells exposed to MC-LR, there was reduced protein phosphatase 1 (PP1) activity, disrupted PP1-mediated PI3K/AKT/FOXO1 signaling, and less expression of follicle maturation-related genes.

Discussion: Using both *in vivo* and *in vitro* murine and human model systems, we provide data suggesting that environmentally relevant exposure to the CyanoHAB toxin MC-LR interfered with gonadotropin-dependent follicle maturation and ovulation. We conclude that MC-LR may pose a nonnegligible risk to women's reproductive health by heightening the probability of irregular menstrual cycles and infertility related to ovulatory disorders. https://doi.org/10.1289/EHP12034

Introduction

Cyanobacterial harmful algal blooms (CyanoHABs) are the excessive growth or bloom of cyanobacteria, which are often referred to as blue-green algae, in both marine and freshwater ecosystems that produce toxins associated with adverse health effects in humans and wildlife animals.[1] Each decade, CyanoHABs increase globally in both severity and frequency, primarily owing to the global temperature rise caused by the climate change and the anthropogenic eutrophication associated with agricultural runoff and urbanization.[2] Microcystins (MCs), the most common class of CyanoHAB toxins,[3] are a family of cyclic heptapeptides with a general structure of cyclo-(D-Ala^1-X^2-D-MeAsp^3-Z^4-Adda^5-D-Glu^6-Mdha^7). With two varying L-amino acids at positions X^2 and Z^4 and modifications in other amino acids, MCs contain nearly 280 different congeners.[4] MCs persist in the environment owing to their high physiochemical stability.[5] Humans are exposed to MCs via drinking water, food, algal dietary supplements, and recreational activities in polluted waters.[6–8] In addition, high-exposure levels of MCs in humans have been reported through contaminated medical solutions, such as the dialysis fluid used in hemodialysis.[9]

With the X^2 and Z^4 positions occupied by leucine (L) and arginine (R), respectively, MC-LR is one of the most common and potent MC congeners. MC-LR has been reported to be hepatotoxic,[10] neurotoxic,[11] and carcinogenic,[12] and several molecular mechanisms underlying these toxicities include the inhibition of protein phosphatases, oxidative stress, and cytoskeletal disruption.[13–15] A key molecular initiating event of MC-LR is the selective inhibition of serine/threonine protein phosphatase 1 or 2A (PP1 or PP2A).[16,17] By interacting with the catalytic subunits of PP1/PP2A through irreversible covalent bonds, MC-LR blocks the access of substrates to PP1/PP2A and inactivates their dephosphorylation activities.[17] The inhibition of PP1/PP2A has been shown to cause an imbalance of substrate protein phosphorylation, including in kinases,[18] cell cycle regulators,[19] and ribonucleoproteins,[20] and their dysregulations can lead to oxidative stress, DNA damage, apoptosis, or tumorigenesis, for example.[21,22]

Address correspondence to Shuo Xiao, 170 Frelinghuysen Rd., Room 406, Piscataway, NJ 08854 USA. Telephone: (848) 445-3729. Email: sx106@pharmacy.rutgers.edu

Supplemental Material is available online (https://doi.org/10.1289/EHP12034).
The authors declare no conflict of interest.
Received 22 August 2022; Revised 28 March 2023; Accepted 19 May 2023; Published 21 June 2023.

Note to readers with disabilities: *EHP* strives to ensure that all journal content is accessible to all readers. However, some figures and Supplemental Material published in *EHP* articles may not conform to 508 standards due to the complexity of the information being presented. If you need assistance accessing journal content, please contact ehpsubmissions@niehs.nih.gov. Our staff will work with you to assess and meet your accessibility needs within 3 working days.

Previously published results in both *in vitro*[23] and in zebrafish[24] models revealed that MC-LR might exhibit endocrine disrupting effects, resulting in reproductive toxicities. Regarding the ovary, the female gonad, MC-LR was found to reduce the numbers of primordial or growing follicles in mice, depending on the exposure route, dose, and treatment window.[25,26] In nonmammalian species, such as zebrafish[27] and medaka fish,[28] MC-LR interfered with oocyte maturation, as well as the interconnections between the oocyte and surrounding somatic cells. Although the observed ovarian toxicities of MC-LR have been related to oxidative stress,[29] endoplasmic reticulum stress,[30] and autophagy[31] in mice, as well as cytoskeletal destruction in porcine oocytes,[32] the underlying mechanism remains poorly understood. To date, no human studies regarding the female reproductive toxicities of MC-LR have been reported. However, with CyanoHABs becoming increasingly prevalent and the lack of routine monitoring of CyanoHAB toxins owing to the lack of federal/state regulatory guidelines, there is an urgent need to determine the ovarian toxicities of MCs and the molecular mechanisms involved.

The ovary is a dynamic female reproductive organ housing various stages of follicles as the functional unit. The earliest staged primordial follicles are activated to develop into the primary, secondary, and antral follicles for maturation and ovulation until menopause.[33] The early phase of follicle development from the primordial to the secondary stage is largely gonadotropin independent; in contrast, the progression of the late phase requires follicle-stimulating hormone (FSH) to support an early antral follicle to the preovulatory stage to reach maturation and become ready for ovulation.[34] Central to FSH-dependent follicle maturation is the activation of the cyclic adenosine monophosphate/protein kinase A (cAMP/PKA) and phosphatidylinositol 3-kinase/protein kinase B/forkhead box protein O1 (PI3K/AKT/FOXO1) signaling pathways and their cross-talk in the granulosa cells of early antral follicles.[35,36] The cross-talk involves the following key events. FSH activates PKA, which phosphorylates the regulatory subunit of PP1 at Ser^{668} for activation. Activated PP1 promotes the dephosphorylation of inhibitory serine residues (Ser^{318}, Ser^{346}, Ser^{612}, and Ser^{789}) of insulin receptor substrate 1 (IRS1), permitting the activation of insulin-like growth factor (IGF)-dependent PI3K/AKT/FOXO1 signaling.[36,37] The activation of this FSH/PP1-dependent signaling cascade up-regulates a suite of genes that are critical for ovarian hormone secretion and follicle maturation.

Because MC-LR selectively inhibits the phosphatase activity of PP1,[16] and PP1 critically mediates FSH-dependent follicle maturation, we hypothesize that MC-LR inhibits PP1 in granulosa cells to disrupt follicle maturation and associated female reproductive outcomes. In the present study, we aimed to test this hypothesis and investigate the ovarian toxic effects and mechanisms of MC-LR using *in vivo* mouse exposure models, a three-dimensional (3D) *in vitro* follicle culture model, and *in vitro* culture of human primary granulosa cells.

Materials and Methods

Animals

All animal procedures in this study were performed according to the National Institutes of Health *Guide for the Care and Use of Laboratory Animals*[38] and were approved by the Rutgers University Institutional Animal Care and Use Committee. The CD-1 mouse breeding colony (Envigo) was housed in a temperature- and humidity-controlled animal facility at Rutgers with a 12-h light/dark cycle and provided with food and water *ad libitum*. Female mice were checked daily for the birth of pups to ensure accuracy of the date of birth recorded. Both male and female pups were weaned on postnatal day 20 and females were housed in groups of 3–5 mice per cage.

Long-Term Low-Dose Oral Exposure to MC-LR in Vivo

In this study, we administered MC-LR (item no. 10007188; Cayman Chemicals) to 4-wk-old young adult CD-1 female mice by oral gavage at 10 μg/kg per day for 6 wk to recapitulate the exposure to MC-LR in humans. We chose oral gavage because humans are primarily exposed to CyanoHAB toxins, including MC-LR, through oral ingestion.[6] The MC-LR exposure dose of 10 μg/kg per day and the treatment duration of 6 wk were selected based on two previous key studies that demonstrated liver toxicities of MC-LR in rodents.[39,40] In the first study, by Heinze et al., the authors examined the changes of liver weight, histology, and serum enzymes; the lowest observed adverse effect level of MC-LR was found to be 50 μg/kg per day in a 4-wk rat study, with the no observed adverse effect level (NOAEL) estimated as 17 μg/kg per day to be used in risk assessment.[39] In the second study, by Fawell et al., the authors investigated the pathological changes of the liver; the NOAEL was determined as 40 μg/kg per day in a 13-wk mouse study.[40]

The NOAELs obtained from these two studies were used as the basis to calculate the reference doses (RfDs) of 50 ng/kg per day and 40 ng/kg per day for the derivation of drinking water health advisories of 1.6 μg/L and 1 μg/L for adults by the U.S. Environmental Protection Agency (EPA; EPA-820r15100)[41] and the World Health Organization (WHO; WHO-HEP/ECH/WSH/2020.6),[42] respectively. The study in mice was also used as the basis of the RfD of 10 ng/kg per day in deriving the recreational health advisory of 2 μg/L by the New Jersey Department of Environmental Protection (NJDEP).[43] Indeed, the human estimated daily intake (EDI) of MC-LR in the real world has been reported to be ∼25.68 ng/kg per day in residents who lived in the townships located in a joint area of the Yangtze River and the Wu River in China that provided drinking water and served as an aquatic food resource but had various degrees of CyanoHAB contamination.[44] Based on the standard body weight of 80 kg and the daily drinking water intake volume of 2.4 L/d given in the U.S. EPA *Exposure Factors Handbook*,[45] the EDI of 25.68 ng/kg per day is equivalent to exposure through drinking water containing MC-LR at 0.86 μg/L for a young adult woman, which is similar to the U.S. EPA and the WHO guidance values.

Given that the human RfDs of 10–50 ng/kg per day established by regulatory agencies for development of drinking water guidance based on the NOAEL of 17–40 μg/kg per day in rodents, the real-world human exposure level of ∼25.68 ng/kg per day, and the high proliferation of cyanobacteria during peak bloom seasons that makes CyanoHAB toxin levels 10 to >1,000 times higher than the WHO/U.S. EPA standards,[46] the *in vivo* dose (10 μg/kg per day) we used here is considered environmentally relevant to humans. Specifically, CD-1 female mice at 4-wk-old ($n = 5$ per group) were treated with 1× phosphate-buffered saline (PBS) or MC-LR at 10 μg/kg via daily oral gavage for 6 wk. MC-LR was dissolved in 1× PBS and stored at −20°C. During the vehicle and MC-LR treatment period, a daily oral gavage of 100 μL of 1× PBS or MC-LR solution was performed using a straight 20-G stainless steel animal feeding needle with a 2-mm ball (Pet Surgical). The mouse body weights were measured and recorded daily before the vehicle or MC-LR administration (Figure 1A).

Estrous Cyclicity Examination

In the last 2-wk treatment window, the estrous cycle of vehicle- or MC-LR–treated mice was determined by daily vaginal smear. The vaginal cells were flushed by introducing 80 μL of 1× PBS through multiple pipetting, and the stage of estrous cycle

was determined by the microscopic examination of vaginal cell cytology and the appearance and proportion of leukocytes, cornified epithelial cells, and nucleated epithelial cells.

Ovarian Histology and Counting of Follicles and Corpora Lutea

At the end of the 6-wk treatment, the mice were sacrificed by carbon dioxide (CO_2) inhalation on diestrus, which was determined by vaginal smear, and the ovaries were harvested. We collected ovaries on diestrus to minimize the potential influence of ovarian hormonal changes on counting the various stages of follicles and corpora lutea (CL). The harvested ovaries were fixed in Shandon Formal-Fixx 10% Neutral Buffered Formalin solution (ThermoFisher Scientific), embedded in paraffin, and serially sectioned at 5 μm with an RM2165 microtome (Leica Microsystems). The ovarian histology and counting of follicles and CL were performed as we have previously described.[47] Briefly, every fifth ovarian section throughout each entire ovary was stained with hematoxylin and eosin (H&E; ThermoFisher Scientific), and the counting of follicles and CL was performed blindly. A primordial follicle was defined as a central oocyte surrounded by single layer of squamous pregranulosa cells. A primary follicle was characterized as an oocyte surrounded by one layer of cuboidal granulosa cells. A secondary follicle was defined as an oocyte surrounded by two or more layers of cuboidal granulosa cells with no visible antrum. An antral follicle was identified as an oocyte surrounded by five or more layers of granulosa cells with a clearly defined antrum. Meanwhile, considering the orientation of the sectioned follicles, a follicle with an oocyte surrounded by more than five layers of granulosa cells with no visible antrum also was defined as an antral follicle. Late-stage antral follicles or preovulatory follicles were defined as type 7 or 8 follicles, with a single antral cavity and formed cumulus oophorus or stalk, according to the classification of Pedersen and Peters.[48] Atretic follicles were characterized by the appearance of >10% of pyknotic granulosa cells surrounding with or without degenerated oocytes. CL were identified by hypertrophic luteal cells and highly vascularized structures between luteal cells. To avoid repeated counting of CL, when a CL was present for the first time in an ovarian section, it was marked and tracked in the following sections until it disappeared. This procedure was repeated for each CL, and the total number of CL in each ovary was recorded.

Mouse Superovulation, Acute MC-LR Exposure, and Oocyte Collection

An *in vivo* mouse superovulation model was used to investigate the toxic effects and mechanisms of MC-LR on gonadotropin-dependent follicle maturation and ovulation. Three MC-LR exposure regimens were performed to distinguish whether MC-LR interferes with FSH-dependent follicle maturation or luteinizing hormone (LH)-dependent follicle ovulation, including the first exposure regimen covering both windows of follicle maturation and ovulation (Figure 2A), the second exposure regimen covering the ovulation window only (Figure 3A), and the third exposure regimen covering the FSH-dependent follicle maturation window only (Figure 3B). For the first exposure regimen, 21-d-old CD-1 female mice were treated with 1× PBS ($N=9$) or 10 μg/kg MC-LR ($N=10$) through intraperitoneal (IP) injection daily for 5 d (Figure 2A). The MC-LR treatment through IP injection was demonstrated to be ∼30–100 times more potent than oral ingestion in mice.[40] Thus, the IP injection of 10 μg/kg MC-LR likely recapitulated the scenario of accidental acute high-dose (300–1,000 μg/kg) exposure to MC-LR during peak CyanoHAB seasons in human. On day 3, mice from the vehicle and MC-LR treatment groups were IP injected with 5 IU of pregnant mare serum gonadotropin (PMSG; ProSpec) to stimulate early antral follicles to grow to the preovulatory stage to reach maturation. On day 5 (46 h post-PMSG), the mice were IP injected with 5 IU of human chorionic gonadotropin (hCG; Sigma-Aldrich), an LH analog, to trigger the ovulation of preovulatory follicles. The mice were sacrificed by CO_2 inhalation 16 h post-hCG injection on day 6, and oocytes were harvested from the ampulla region of both sides of the oviducts. The numbers of ovulated oocytes and the percentages of metaphase II (MII) oocytes with visible first polar bodies were examined by light microscopy and recorded. The ovaries from hCG-treated mice were collected for ovarian histology and counting of un-ovulated late-stage antral follicles (type 7 and 8).[48]

For the second and third MC-LR exposure regimens, the PMSG and hCG treatment methods were the same as the first exposure regimen. However, the mice were treated only with 1× PBS ($N=12$) or 10 μg/kg MC-LR ($N=14$) through IP injection on day 5 (1 h before hCG injection) for the second exposure regimen (Figure 3A), and the mice were treated with 1× PBS ($N=8$) or 10 μg/kg MC-LR ($N=9$) daily through IP injection on the first 4 d for the third exposure regimen (Figure 3B).

Measurement of the Size of Late-Stage Antral Follicles and Immunohistochemistry

To examine the effects of MC-LR on follicle growth and maturation *in vivo*, CD-1 female mice at 21-d-old were treated with 1× PBS ($N=3$) or MC-LR ($N=4$), as we described in the first exposure regimen except that the mice were not treated with hCG for ovulation induction. Ovaries were collected and processed at the end of day 5 (46 h post-PMSG), and ovarian sections were obtained as described above. We first measured the size of late-stage healthy antral follicles to investigate the effects of MC-LR on follicle growth. To ensure the accuracy of measurements, only the type 7 or 8 antral follicles with a single cavity and formed cumulus oophorus and/or stalk, as well as a clearly visible oocyte nucleus, were included. Collectively, 91–95 antral follicles from 6–8 ovaries in the PBS or MC-LR group were assessed using ImageJ software (version 1.53).[49] The antral follicle diameter was calculated based on the average of two perpendicular measurements from one side to another side of basement membrane per follicle, with the first measurement detecting the widest diameter and the second measurement originating at a right angle from the midpoint of the first measurement.

The ovarian accumulation of MC-LR and the expression of follicle maturation-related protein LH receptor (LHCGR) and pregnancy-associated plasma protein A (PAPPA) were determined by immunohistochemistry (IHC). Ovarian sections were deparaffinized in xylene and rehydrated in graded ethanol baths (100%, 95%, 80%, 70%, and 50%). Antigen retrieval was performed by microwaving slides in 0.01 M sodium citrate medium (pH = 6) for 15 min (min). The slides were then incubated in 3% hydrogen peroxide (ThermoFisher Scientific), followed by incubating in the blocking buffer [2% bovine serum albumin (BSA) diluted in PBS] for 1 h at room temperature (RT). Then the slides were incubated in the specific primary antibody diluted in 2% BSA in PBS for 3 h at 4°C, rinsed using PBS for three times, and incubated with the secondary antibody [1:500, goat antimouse IgG H&L (horseradish peroxidase; HRP), ab6789, or goat antirabbit IgG (HRP), ab6271; Abcam] for 1 h at RT. Moreover, to detect the nonspecific antibody binding of target primary antibodies, the specific primary antibody was replaced by normal rabbit IgG (1:200, #2729S; Cell Signaling Technology). Protein signals were detected using the DAB substrate kit (Abcam) according to the manufacturer's instructions, and counterstaining was performed using hematoxylin. The staining intensities of LHCGR and PAPPA were quantified using ImageJ Fiji software as previously described.[50] Primary

antibody against MC-LR (1:200, NBP2-89072) was purchased from Novus Biologicals. Primary antibodies against PAPPA (1:200, ab203683) and LHCGR (1:200, ab125214) were purchased from Abcam.

Follicle Isolation, Encapsulation, Encapsulated in Vitro *Follicle Growth, and MC-LR Exposure*

Ovaries were removed from 16-d-old CD-1 female mice and multilayered secondary follicles were enzymatically isolated using an enzymatic solution containing Leibovitz's L-15 medium (Gibco) with Liberase TM (30.8 μg/mL; Roche) and DNase I (200 μg/mL; Worthington Biochemicals). Morphologically normal follicles with diameters of 130–160 μm were selected, encapsulated with alginate hydrogel for encapsulated *in vitro* follicle growth (eIVFG), and randomly distributed into different groups, as we have previously described, with minor modifications.[51,52] Briefly, follicles were individually encapsulated in 0.5% alginate hydrogel (Sigma-Aldrich), and the alginate beads containing follicles were incubated in the maintenance media containing minimum essential medium (αMEM Glutamax; Gibco) with 1% FBS for 30 min at 37°C in 5% CO_2.

Follicles encapsulated within the alginate hydrogel were individually cultured in 96-well plates, with each well containing 100 μL of growth media for 6 d at 37°C in a humidified environment of 5% CO_2. The follicle growth media consisted of 50% αMEM Glutamax and 50% F-12 Glutamax supplemented with 3 mg/mL BSA (Fisher Scientific), 1 mg/mL bovine fetuin (Sigma-Aldrich), 5 μg/mL insulin, 5 μg/mL transferrin, and 5 ng/mL selenium (ITS; Sigma-Aldrich), as well as 5 mIU/mL (day 0–4) or 10 mIU/mL (day 4–6) of recombinant human FSH (r-hFSH; from A.F. Parlow, National Hormone and Peptide Program, National Institute of Diabetes and Digestive and Kidney Diseases, Bethesda, MD). During eIVFG, the follicles were treated with MC-LR at various concentrations (0–10 μM) from day 2 to day 6. For the PI3K activator co-treatment experiment from day 2 to day 6 of eIVFG, the follicles were pretreated with PI3K activator 740 Y-P peptide (SelleckChem) for 1 h before the MC-LR treatment, and the follicles were then co-treated with 10 μM MC-LR from day 2 to day 6. For each *in vitro* exposure experiment using eIVFG, the follicles were imaged at each media change to examine follicle survival and assess diameter using an Olympus inverted microscope with a 10× objective (Olympus Optical Co Ltd.). The follicles were considered dead if they had unhealthy-appearing oocytes and/or granulosa cells or if the integrity of the oocyte and somatic cell interface was visibly compromised. The follicle diameter was calculated by averaging two perpendicular measurements from one side to another side of basement membrane per follicle using ImageJ software (version 1.53).[49]

Ovulation Induction in Vitro

Antral follicles from day 6 of eIVFG were removed from the alginate beads by incubating the alginate beads in L15 media containing 1% FBS and 10 IU/mL alginate lyase (Sigma-Aldrich) at 37°C for 10 min. The follicles were then treated with αMEM-based ovulation induction media containing 10% FBS and 1.5 IU/mL hCG (C1063; Sigma-Aldrich) at 37°C in 5% CO_2. At 14 h post-hCG treatment, the follicles were imaged with a 10× objective to examine the follicle rupture and oocyte meiosis. Follicles with a follicular wall broken from one side and an expanded cumulus–oocyte complex were defined as ruptured follicles; follicles with an intact follicular wall were defined as unruptured follicles.

Human Granulosa Cell Culture and MC-LR Treatment

Human luteinizing mural granulosa cells were aspirated during oocyte retrieval from patients undergoing *in vitro* fertilization (IVF) at the Colorado Center for Reproductive Medicine. To eliminate the confounding effects of disease-associated dysfunctional granulosa cells, samples were collected from egg donors with male factors of infertility as the reason for IVF who signed the consent forms to donate discarded biological materials for research with institutional review board approval (Western Institutional Review Board no. 20142468). After the retrieval of the cumulus–oocyte-complex, luteinizing mural granulosa cells were collected from residual follicular aspirates and washed three times with 1× PBS. To decrease intervariability between women, luteinizing granulosa cells from three different patients were pooled together. ACK lysing buffer (ThermoFisher Scientific) was used to lyse the red blood cells. Granulosa cells were separated from the blood cells using a Percoll gradient (P4937; Sigma-Aldrich). Purified cells were then plated in 24-well plates (100,000 cells/well) and cultured in Dulbecco's Modified Eagle Medium/Nutrient Mixture F-12 (DMEM/F12; Gibco) supplemented with 10% FBS (Sigma-Aldrich) and 1% penicillin/streptomycin (Gibco) at 37°C in a humidified atmosphere of 5% CO_2. After 36 h, the medium was replaced with DMEM/F12 medium containing 1% penicillin/streptomycin, 10 mIU/mL FSH, and MC-LR at 0 or 10 μM. Granulosa cells were harvested 24 h posttreatment for PP1 and PP2A phosphatase activity measurement, western blotting, and reverse transcription–quantitative polymerase chain reaction (RT-qPCR).

Hormone Measurements

To investigate the effects of MC-LR on ovarian steroidogenesis, the concentrations of 17β-estradiol (E2) and testosterone (T) in the conditioned culture media from day 6 of eIVFG was measured using E2 and T enzyme-linked immunosorbent assay (ELISA) kits (Cayman Chemical Company) according to the manufacturer's instructions. To evaluate the effects of MC-LR treatment during the follicle maturation window on the subsequent luteinization, after ovulation induction, hCG-treated follicles were continuously cultured for 48 h to allow for luteinization and progesterone secretion. The conditioned culture media was collected to measure the concentration of progesterone (P4) using the progesterone ELISA kit (Cayman Chemical Company) according to the manufacturer's instructions. The reportable ranges of the E2, T, and P4 assays were 0.61–10,000, 3.9–500, and 7.8–1,000 pg/mL, respectively. The interassay coefficients of variability and intra-assay coefficients of variability were <10% for all assays.

Quantitative RT-PCR

The total RNA of a single follicle from either *in vivo* or *in vitro* exposure experiment was extracted using the Arcturus PicoPure RNA isolation kit (Applied Biosystems) according to the manufacturer's instructions. The total RNA from a single follicle was then reverse transcribed into complementary DNA using the Superscript III reverse transcriptase with random hexamer primers (Invitrogen) and stored at −80°C. qPCR was performed in a 384-well plate using Power SYBR Green PCR Master Mix (Applied Biosystems) on an ABI ViiA 7 real-time PCR system (Applied Biosystems). The qPCR thermos cycle was programmed for 10 min at 95°C, followed by 40 cycles of 15 s at 95°C and 1 min at 60°C, and finally a melting stage to determine the specificity of primers. The mRNA expression levels of each gene were normalized by the expression of glyceraldehyde-3-phosphate dehydrogenase (*Gapdh*). All primers were synthesized by Integrated DNA Technologies and their sequences used for PCR in this study are shown in the Table S1.

Single-Follicle RNA Sequencing

To investigate the effects of MC-LR on the whole follicular transcriptome, antral follicles treated with vehicle or 10 μM MC-LR

were collected from day 6 of eIVFG for single-follicle RNA sequencing (RNA-seq, GEO number: GSE201806). Total RNA extraction was performed using the Arcturus PicoPure RNA isolation kit (Applied Biosystems) according to the manufacturer's instructions. Next, the library preparation and low-input RNA sequencing were performed on an Illumina NovaSeq PE150 platform by Novogene. High-quality trimmed paired sequencing reads were uploaded into Partek Flow software (version 10.0.22.0121) for data analyses. The potential ribosomal DNA and mitochondrial DNA contaminants were filtered using Bowtie 2. Next, the filtered reads were aligned to the whole mouse genome assembly mm10 using the HISAT 2 aligner. Raw read counts were achieved by quantifying aligned reads to Ensembl Transcripts release 99 using the Partek expectation–maximization algorithm and then normalized based on the transcripts per million method. Differential expression analysis was performed using the DEseq2(R) and genes with an absolute fold change >1.5 and a false discovery rate (FDR) adjusted $p < 0.05$ were recognized as differentially expressed genes (DEGs).

PP1 and PP2A Phosphatase Activity Measurement

The phosphatase activities of PP1 or PP2A in vehicle- or MC-LR–treated murine follicles and human primary granulosa cells were measured by using the RediPlate 96 EnzChek Serine/Threonine Phosphatase Assay Kit (ThermoFisher Scientific) according to the manufacturer's protocol. Briefly, immature mouse follicles were cultured using eIVFG and treated with vehicle or 10 μM MC-LR from day 2 to day 6 as we described above. On day 6 of eIVFG, 25–30 follicles were pooled together in each treatment group and lysed with the M-PER Mammalian Protein Extraction Reagent (ThermoFisher). The protein concentrations of follicle lysates were then determined using the Bradford protein assay kit (Abcam). Next, equal amounts of proteins (8 μg) in each group were used to determine the phosphatase activity of PP1 and PP2A. The plate containing loaded proteins was incubated at RT and the fluorescence was then measured at multiple time points on a Spectramax M3 microplate reader (Molecular Devices) with excitation and emission wavelengths of 355 and 460 nm, respectively.

Western Blotting

Twenty to 25 mouse follicles or ∼20,000 human primarily granulosa cells in each group were pooled together and lysed in ice-cold Laemmli sample buffer (Bio-Rad) containing the protease and phosphatase inhibitor cocktail (ThermoFisher Scientific), and the lysate was separated on 12% acrylamide/bisacrylamide gels. Proteins were transferred to a 0.45-μm nitrocellulose blotting membrane (GE Health care Life Science). After blocking with 5% BSA in Tris-buffered saline with 0.1% Tween-20, the membranes were incubated with specific primary antibodies overnight at 4°C and appropriate HRP-conjugated secondary antibodies at a dilution of 1:2,000 for 1 h at RT. The protein was detected using Pierce Enhanced Chemiluminescence (ECL) Western Blotting Substrate Kit (ThermoFisher Scientific) according to the manufacturer's instructions. Next, the ECL signals were captured by X-ray film (Fuji X-ray film) and the western blotting bands were quantified using ImageJ software (version 1.53).[49] The antibodies used included anti-β-actin (1:1,000, ab6276; Abcam), anti-PCNA (1:1,000, ab2426; Abcam), anti-γH2AX (phospho Ser139) (1:1,000, ab26350; Abcam), anti-FOXO1A (phospho S253) (1:1,000, ab259337), anti-AKT (1:1,000, 9272S; Cell Signaling Technology), anti-AKT (phospho T308) (1:1,000, ab8933; Abcam), anti-AKT (phospho S473) (1:1,000, ab81283; Abcam), and anti-MC-LR (1:1,000, NBP2-89072; Novus Biologicals).

Benchmark Dose Modeling

The frequentist benchmark dose (BMD) modeling approach was used to determine the *ex vivo* point of departure of MC-LR from the dichotomous concentration–response data on failed follicle rupture and oocyte meiosis observed in MC-LR–treated follicle cultures. The U.S. EPA Benchmark Dose Software (BMDS) tool (version 3.1.2) was used.[53] The 10% extra risk of failed follicle rupture or completion of oocyte meiosis I was set as the benchmark response (BMR_{10}) level to derive the benchmark concentration (BMC_{10}) and the corresponding 95% lower confidence limit ($BMCL_{10}$). The default recommended model selection and restriction was used—the Gamma, Log-Logistic, Multistage and Weibull models were run restricted, and the Log-Probit and Dichotomous Hill, the Logistic, Probit and Quantal Linear models were run unrestricted. Selection of the best models was used to determine BMC and BMCL, following the U.S. EPA-recommended guideline.

Statistical Analyses

Statistical analysis was performed using GraphPad Prism (version 9; GraphPad Software). Two-way analysis of variance (ANOVA) with Bonferroni's post-test was used to compare mouse body weight. Student's *t*-tests were used to compare differences between two groups for the numbers of days on various estrous cycle stages, follicle and CL numbers, numbers of ovulated oocytes, MII oocyte percentages, follicle diameters, and expression of follicle maturation or ovulation-related genes. One-way ANOVA followed by a Tukey's multiple comparisons test was performed to analyze the follicle growth, survival, follicle rupture, hormone concentration, and expression of follicle maturation-related genes when comparing multiple groups. A $p < 0.05$ was considered statistically significant.

Results

Effect of Long-Term Low-Dose Oral Exposure to MC-LR on Number of CL

CD-1 female mice (4-wk-old) were exposed to 1× PBS or 10 μg/kg MC-LR via daily oral gavage for 6 wk (Figure 1A). Animals exposed to MC-LR did not exhibit any significant differences in general health, body weight, or the pattern of weight gain compared with control animals (Figure 1B; Table S2). The vaginal smear data in the last 2 wk of treatment revealed comparable estrous cyclicity between the control and MC-LR treatment groups (Figure 1C; Table S3).

At the end of the 6-wk exposure, ovaries from MC-LR–treated mice had histological morphology and numbers of follicles at all stages that were comparable to the control group (Figure 1D,E; Table S4), including primordial follicles (688 ± 89 vs. 667 ± 144), primary follicles (300 ± 67 vs. 357 ± 80), secondary follicles (148 ± 45 vs. 146 ± 35), antral follicles (16 ± 5 vs. 16 ± 5), and atretic follicles (79 ± 21 vs. 92 ± 8). However, there were nearly 50% fewer CL, a mass of cells that is formed from postovulatory follicular somatic cells, in MC-LR–treated ovaries than in the control group (7 ± 3 vs. 12 ± 4, Figure 1D,F; Table S5).

Effect of in Vivo *Acute Exposure to MC-LR on Ovulation*

Given the well-characterized inhibitory effect of MC-LR on PP1, a protein phosphatase key to the activation of the PI3K/AKT/FOXO1 signaling that underpins FSH-dependent follicle maturation,[36,37] we hypothesized that MC-LR perturbs the maturation of preantral follicles toward the preovulatory stage to block the LH-induced ovulation and luteinization. To test the hypothesis, we first used the *in vivo* mouse superovulation model to examine the possible adverse effects of MC-LR on two gonadotropin-

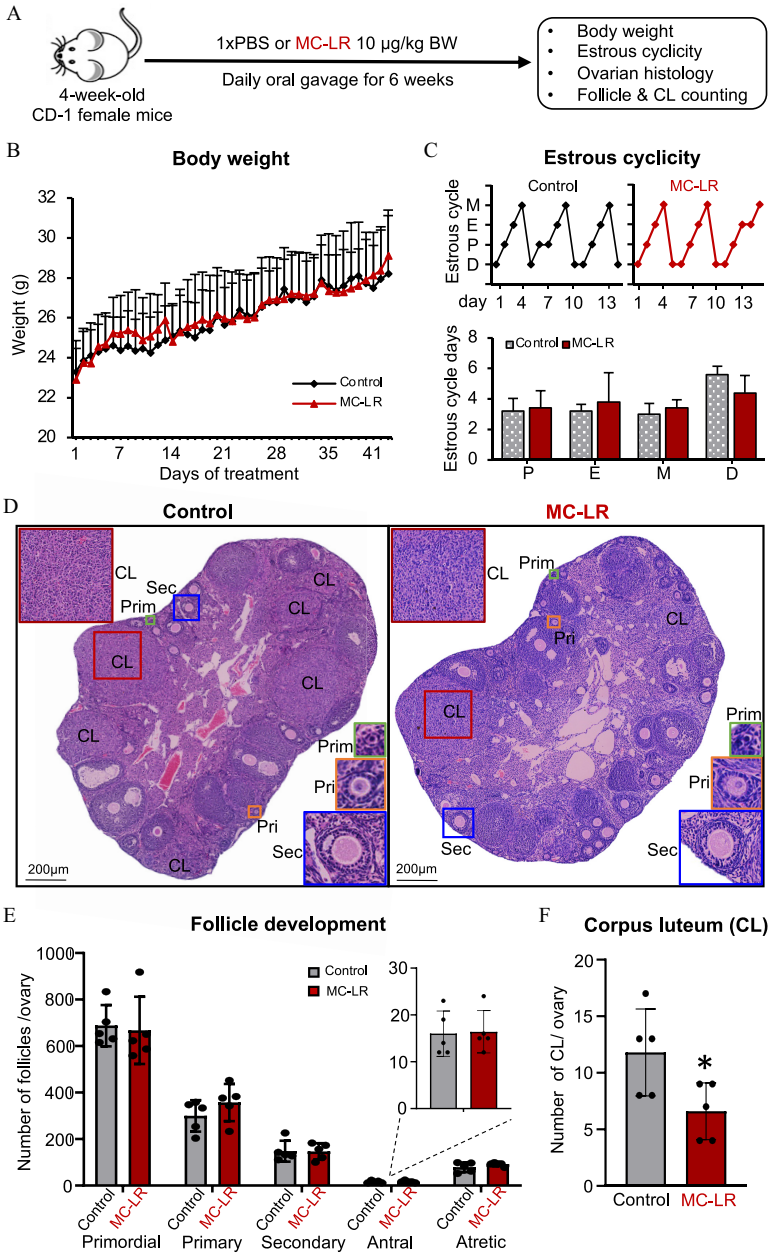

Figure 1. Assessment of mouse body weight, ovarian cyclicity, and folliculogenesis following a long-term, low-dose oral exposure to MC-LR. (A) The schematic of long-term MC-LR oral exposure *in vivo*. $N = 5$ mice in each group. (B) Effect of MC-LR on mouse body weight during the 6-wk treatment. Average daily body weight in 1× PBS- or MC-LR–treated mice. (C) Representative 14-d estrous cyclicity (top) and the numbers of days in each estrous cycle stage (bottom) in the last 2 wk of 1× PBS or MC-LR treatment. (D) Representative ovary histological images after 6-wk 1× PBS or MC-LR treatment. Red squares indicate corpora lutea (CL); green squares indicate primordial follicles (Prim); orange squares indicate primary follicles (Pri); and blue squares indicate secondary follicles (Sec). (E) Total numbers of various stages of follicles per ovary in 1× PBS- or MC-LR–treated mice. (F) Total numbers of CL per ovary in 1× PBS- or MC-LR–treated mice. $N = 5$ mice in each group. Data were analyzed with two-way ANOVA with Bonferroni's post-test (B) and Student's *t*-test (C,E, F). Bidirectional error bars represent mean ± standard deviation; $^{*}p < 0.05$. Data in (B,C,E,F) are also presented in Tables S2–S5, respectively. Note: ANOVA, analysis of variance; D, diestrus; E, estrus; M, metestrus; MC-LR, microcystin-LR; P, proestrus; PBS, phosphate-buffered saline.

dependent ovarian events: FSH-dependent follicle maturation and LH-dependent follicle ovulation. As shown in Figure 2A, 21-d-old CD-1 female mice were treated with 1× PBS or 10 μg/kg MC-LR through daily IP injection for 5 d. The mice were then treated with PMSG on day 3 to stimulate follicle maturation followed by the injection of hCG on day 5 to induce follicle ovulation.

Results showed that at 16 h post-hCG injection on day 5, there were significantly fewer oocytes harvested from both sides of oviducts in MC-LR–treated mice than in the control group (25 ± 10 vs. 38 ± 8; Figure 2B,C; Table S6). For these ovulated oocytes, there were comparable percentages of MII oocytes (97.1% vs. 98.5%) in the control and MC-LR groups (Figure 2D; Table S7). Histological staining showed that, compared with the control group, there were significantly more late-stage antral follicles (type 7 and 8) that did not ovulate or rupture in the ovaries of MC-LR–treated mice (16 ± 4 vs. 9 ± 2; Figure 2E,F; Table S8).

Effect of MC-LR on Gonadotropin-Dependent Follicle Maturation and Ovulation

To distinguish whether MC-LR interferes with follicle maturation that causes a secondary ovulation defect or it directly inhibits

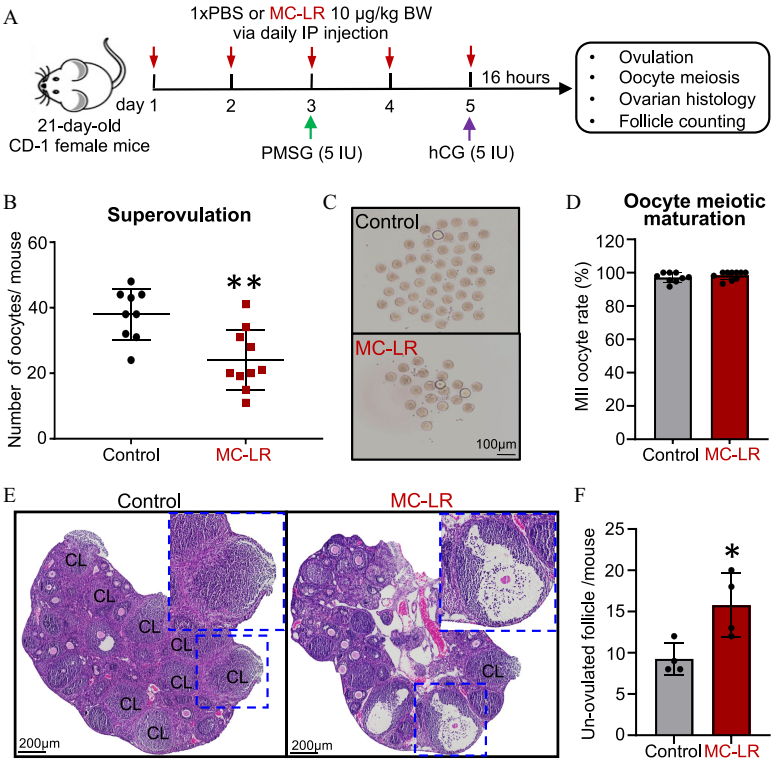

Figure 2. Effects of acute exposure to MC-LR on follicle ovulation. (A) The schematic of intraperitoneal treatment of 1× PBS ($N = 9$) or 10 μg/kg MC-LR ($N = 10$) in a mouse superovulation model. (B) Numbers and (C) representative images of ovulated oocytes from mice treated with 1× PBS or MC-LR. (D) Percentages of ovulated MII oocytes in mice treated with 1× PBS or MC-LR. (E) Representative ovarian histological images after ovulation induction in 1× PBS- or MC-LR–treated mice. Blue dash squares indicate newly formed corpora lutea (CL) or un-ovulated late-staged antral follicles in 1× PBS- or MC-LR–treated mouse ovaries, respectively. (F) Total numbers of un-ovulated late-staged antral follicles per mouse in 1× PBS- or MC-LR–treatment groups. $N = 4$ mice or 8 ovaries were randomly selected in each group for the histological staining and counting of un-ovulated follicles. Data were analyzed with Student's *t*-test (B,D,F). Bidirectional error bars represent mean ± standard deviation; $^{*}p < 0.05$ and $^{**}p < 0.01$. Data in (B,D,F) are also presented in Tables S6–S8, respectively. Note: hCG, human chorionic gonadotropin; IP, intraperitoneal; MC-LR, microcystin-LR; MII, metaphase II; PBS, phosphate-buffered saline; PMSG, pregnant mare serum gonadotropin.

ovulation per se, we next performed an *in vivo* exposure experiment involving two different MC-LR treatment regimens. The mice in exposure regimen 1 were treated with a single IP injection of 1× PBS or 10 μg/kg MC-LR at 1 h before hCG injection and ovulation induction (Figure 3A; Table S9). There were comparable numbers of ovulated oocytes (40 ± 10 vs. 42 ± 12) and percentages of MII oocytes (94 ± 3 vs. 95 ± 3%) between vehicle- and MC-LR–treated mice. In exposure regimen 2, the mice were treated with multiple IP injections of 1× PBS or 10 μg/kg MC-LR during the follicle maturation window only (Figure 3B; Table S10). There were significantly fewer ovulated oocytes from MC-LR–treated mice than the control group (24 ± 9 vs. 36 ± 11), but the percentages of MII oocytes were comparable (92 ± 6 vs. 95 ± 3%).

MC-LR Accumulation in the Ovary and Its Impacts on Follicle Maturation Mediators

To decipher the underlying mechanism of failed follicle maturation caused by MC-LR, we performed the same exposure experiment as shown in Figure 3B. Mice were sacrificed 46 h post-PMSG injection without hCG treatment. No obvious nonspecific antibody binding was detected in the negative control ovarian sections using normal rabbit IgG (Figure S1). IHC results showed that MC-LR accumulated in the ovary, including stroma cells, theca cells, and granulosa cells in antral follicles (Figure 4A). Ovaries from vehicle- and MC-LR–treated mice had comparable diameters of large antral follicles (type 7 and 8), implying that MC-LR treatment did not affect follicle growth and survival (Figure 4B,C; Table S11).

We further isolated large antral follicles from the ovaries of PBS- or MC-LR–treated mice and performed single-follicle RT-qPCR to examine the expression of several genes critical for the FSH-induced follicle maturation. The specific genes, their full names, functions in follicle maturation, and references are listed in Table S12. The mice exposed to MC-LR had significantly lower expression of several of these genes, including *Inha*, *Comp*, *Lhcgr*, and *Pappa* (Figure 4D; Table S13). Consistent with RT-qPCR results, IHC revealed that both LHCGR and PAPPA were remarkably lower in the granulosa cells of antral follicles in MC-LR–treated ovaries (Figure 4E,F; Table S14 and S15).

Effects of MC-LR Exposure in a 3D in Vitro *Mouse Follicle Culture Model*

To further investigate the mechanisms of defective follicle maturation caused by MC-LR and also subsequent reproductive outcomes such as ovulation, luteinization, and ovarian steroidogenesis, we used our established 3D *in vitro* follicle culture model, eIVFG, to perform an *in vitro* exposure experiment. We have previously demonstrated that eIVFG recapitulates the hallmark events of follicle maturation, hormone secretion, ovulation, and luteinization.[51] This *in vitro* exposure regimen also enables us to confirm the direct ovarian impact of MC-LR. During eIVFG, immature mouse follicles were treated with MC-LR at 0, 0.1, 1, and 10 μM from day 2 to day 6, to recapitulate MC-LR exposure during FSH-dependent follicle maturation. Follicles from all treatment groups had comparable morphology (Figure 5A) and survival rates (Figure 5B; Table S16),

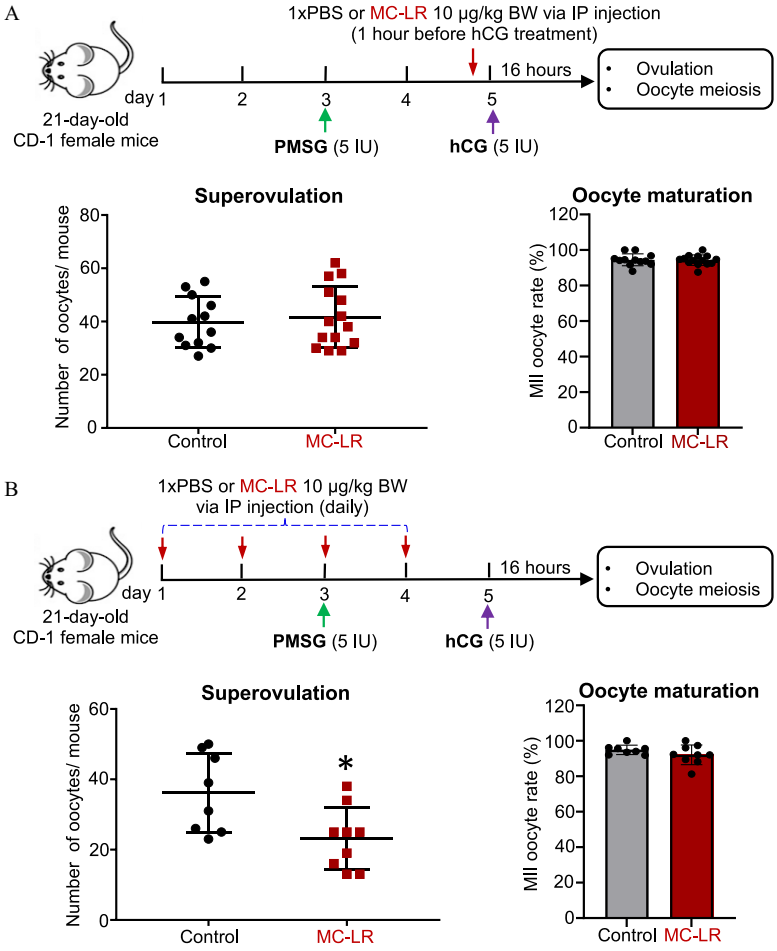

Figure 3. Effects of acute MC-LR exposure during ovulation window and follicle maturation window on follicle ovulation. (A) The schematic of acute MC-LR exposure during the ovulation window. CD-1 female mice at 21-d-old were intraperitoneally treated with 1× PBS ($N = 12$) or 10 μg/kg MC-LR ($N = 14$) at 1 h before hCG injection, and the numbers of ovulated oocytes and percentages of MII oocytes at 16 h post-hCG injection. (B) The schematic of acute MC-LR exposure during the follicle maturation window. CD-1 female mice (21-d-old) were intraperitoneally treated with 1× PBS ($N = 8$) or 10 μg/kg MC-LR ($N = 9$) from day 1 to day 4, and the numbers of ovulated oocytes and percentages of MII oocytes at 16 h post-hCG injection were determined. Data were analyzed with Student's *t*-test (A,B). Bidirectional error bars represent mean ± standard deviation; $^{*}p < 0.05$. Data in (A,B) are also presented in Tables S9 and S10, respectively. Note: hCG, human chorionic gonadotropin; IP, intraperitoneal; MC-LR, microcystin-LR; MII, metaphase II; PBS, phosphate-buffered saline; PMSG, pregnant mare serum gonadotropin.

and follicles from all groups were able to grow from the secondary stage to the antral stage with comparable follicle size (Figure 5C; Table S17). The concentrations of E2 and T in the conditioned media were similar between the different groups (Figure 5D,E; Table S18 and S19).

We next treated grown antral follicles with hCG on day 6 of eIVFG to induce ovulation *in vitro*. The mice exposed to MC-LR demonstrated inhibited follicle ovulation, particularly the follicle rupture, and this effect appeared to be concentration dependent (Figure 5F,G; Table S20). In the control and 0.1 μM MC-LR treatment groups, nearly 100% follicles ruptured and ovulated MII oocytes in response to hCG stimulation; however, in the 1 and 10 μM MC-LR treatment groups, only 77.5 ± 7.8% and 11.9 ± 3.2% follicles ruptured, and 76.9 ± 4.0% and 36.4 ± 7.9% oocytes were at the MII stage (Figure 5F,G; Table S20). Given that the failure of follicle rupture and oocyte meiosis during ovulation is directly associated with increased risks of irregular female reproductive cycle and infertility, we derived the *in vitro* BMC_{10} and $BMCL_{10}$ of MC-LR for the 10% extra risk of failure in both responses. Using the U.S. EPA BMDS tool, the best model for the follicle rupture response was quantal linear, which gave a BMC_{10} of 0.518 μM and $BMCL_{10}$ of 0.377 μM (Figure S2A). The best model for the resumption and completion of oocyte meiosis I was Log-Probit, which gave a BMC_{10} of 0.595 μM and $BMCL_{10}$ of 0.14 μM (Figure S2B). Follicles treated with hCG were next cultured for 48 h to allow for luteinization. Follicles treated with 10 μM MC-LR during the follicle maturation window had significantly lower concentrations of progesterone in the conditioned media, suggesting defective luteinization and progesterone synthesis (Figure 5H; Table S21).

We next used the same exposure regimen with vehicle or 10 μM MC-LR during the follicle maturation window to investigate the mechanisms of MC-LR on follicle maturation (Figure 6A). We first collected follicles on day 6 of eIVFG for single-follicle RT-qPCR to examine the expression of follicle maturation-related genes listed in Table S12. Follicles treated with vehicle had significantly increased expression of all examined genes from day 0 to day 6 (Figure 6B, black dots; Table S22), in support of eIVFG preserving molecular signatures of FSH-dependent follicle maturation. In MC-LR–treated follicles, however, the expression of all these genes were significantly lower on day 6 compared with the control group (Figure 6B, red dots vs. black dots; Table S22); particularly for

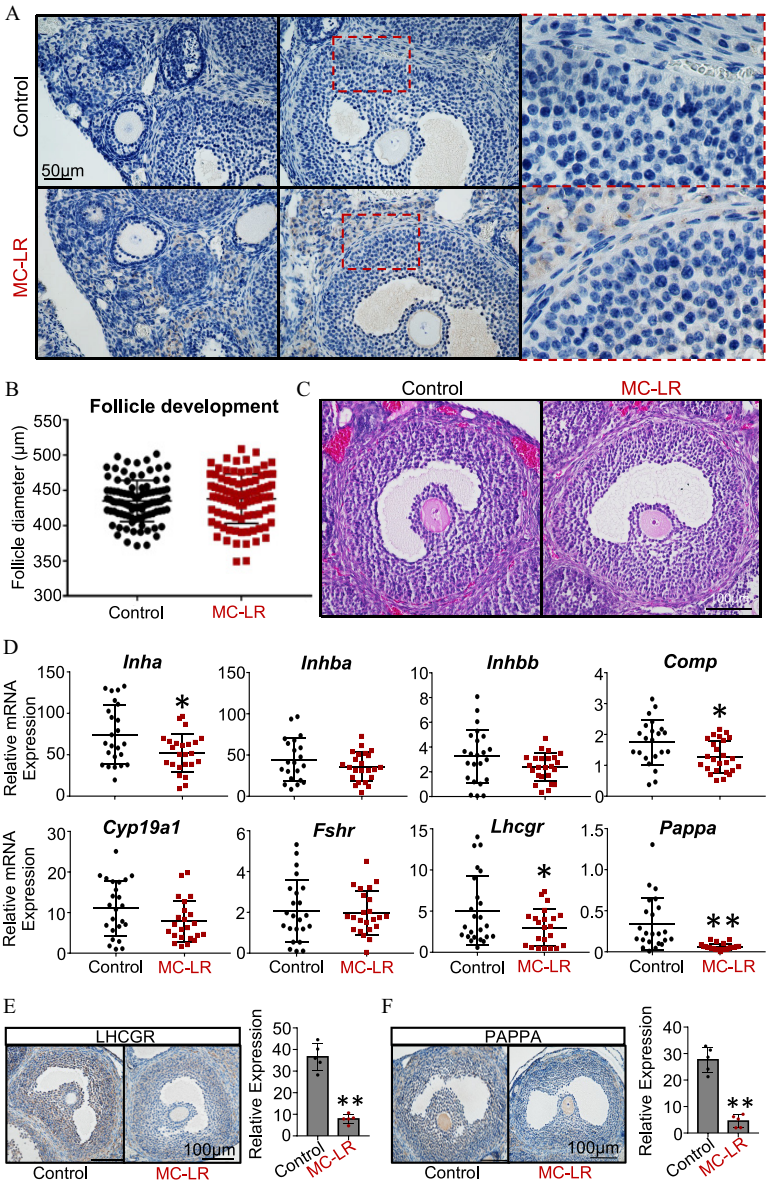

Figure 4. MC-LR accumulation in the ovary and examination of follicle maturation in response to MC-LR exposure. (A) Ovarian accumulation of MC-LR examined by immunohistochemistry (IHC). (B) Diameters of late-staged antral follicles isolated from mice treated with 1× PBS ($N = 91$ follicles from 6 ovaries) and MC-LR ($N = 95$ follicles from 8 ovaries). (C) Representative histological images of late-staged antral follicles in ovaries from 1× PBS- or MC-LR–treated mice. (D) Expression of follicle maturation-related genes in isolated large antral follicles from 1× PBS- or MC-LR–treated mice. $N = 24$ and 25 follicles were isolated from 5 mice treated with 1× PBS and MC-LR, respectively. Expression and quantification of (E) LHCGR and (F) and PAPPA in late-staged antral follicles in 1× PBS- or MC-LR–treated ovaries examined by IHC. Data were analyzed with Student's *t*-test (B,D,E,F). Bidirectional error bars represent mean ± standard deviation; $^{*}p < 0.05$ and $^{**}p < 0.01$. Data in (B,D–F) are also presented in Tables S11, S13–S15, respectively. Note: MC-LR, microcystin-LR; PBS, phosphate-buffered saline.

Pappa and *Lhcgr*, expression were 5.36- and 5.84-fold lower, respectively. For *Inha*, *Cyp19a1*, and *Inhbb*, lower expression was even observed starting on day 4 (Figure 6B; Table S22). To determine whether the inhibitory effect of MC-LR on these follicle maturation-related genes was related to granulosa cells, we performed another *in vitro* exposure and isolated mural granulosa cells from cultured follicles on day 6 of eIVFG for RT-qPCR, which consistently showed the significant lower expression of all follicle maturation-related genes compared with control (Figure 6C; Table S23).

We next stimulated vehicle- and MC-LR–treated follicles from day 6 of eIVFG with hCG for ovulation induction. Given that many ovulatory genes were highly induced at 4 h post-hCG in both *in vivo* and *in vitro* models,[54] we collected follicles at 4 h for RT-qPCR to examine the expression of several established ovulation genes (Figure 6D; Table S24 and S25). The specific genes, their full names, and functions in ovulation are listed in Table S24. All these ovulatory genes were expressed at much lower levels in follicles treated with MC-LR during the follicle maturation window (Figure 6D; Table S25).

Single-Follicle RNA-Seq Analysis in Response to MC-LR Exposure in Vitro

To further characterize the effects of MC-LR on FSH-dependent follicle maturation in an unbiased manner, we performed the same vehicle and MC-LR exposure as shown in Figure 6A and collected follicles on day 6 of eIVFG for single-follicle RNA-seq

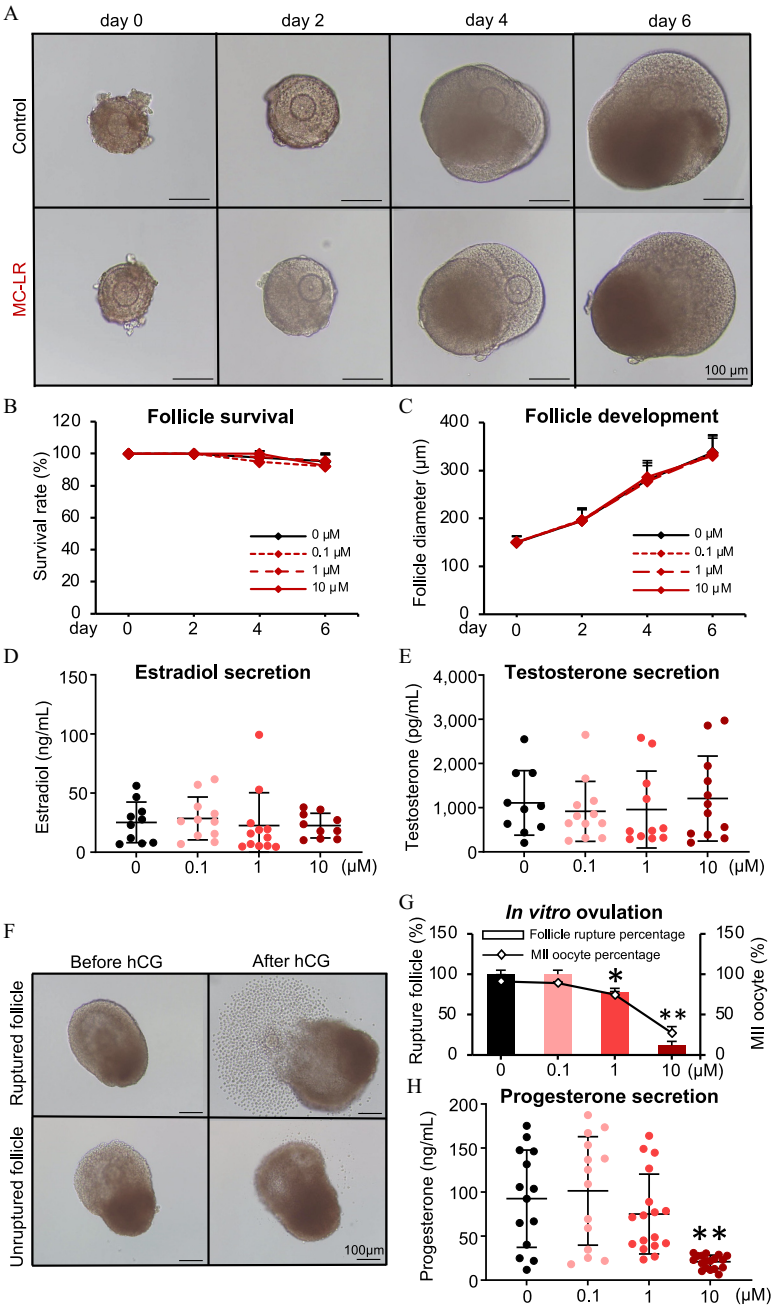

Figure 5. Effects of MC-LR on follicle maturation, ovarian steroidogenesis, ovulation, and luteinization *in vitro*. (A) Representative images of follicles treated with vehicle or 10 μM MC-LR during eIVFG. The (B) survival rates and (C) diameters of follicles treated with various concentrations of MC-LR. $N = 13–14$ follicles in each group per replicate, and three replicates were included. Concentrations of (D) estradiol and (E) testosterone in the conditioned follicle culture media. $N = 10–12$ follicles in each group. (F) Representative follicle images before and after hCG treatment, with vehicle- or MC-LR–treated follicles stimulated with 1.5 IU/mL hCG on day 6 of eIVFG for ovulation induction. (G) Percentages of ruptured follicles and MII oocytes in various treatment groups. (H) Concentrations of progesterone in the conditioned follicle culture media after hCG-stimulated follicles were cultured for 48 h to allow for luteinization. $n = 14–17$ follicles in each group. Data were analyzed with one-way ANOVA followed by a Tukey's multiple comparisons test (B–E,G,H). Bidirectional error bars represent mean ± standard deviation; $^{*}p < 0.05$ and $^{**}p < 0.01$. Data in (B–E,G,H) are also presented in Tables S16–S21, respectively. Note: ANOVA, analysis of variance; eIVFG, encapsulated *in vitro* follicle growth; hCG, human chorionic gonadotropin; MC-LR, microcystin-LR; MII, metaphase II.

analysis. High-quality sequencing data were generated from single follicles (Figure S3; Table S26) and thousands of DEGs were identified. Principal component analysis separated vehicle- and MC-LR–treated follicles into two distinct clusters (Figure 7A). There were 3,368 DEGs (absolute fold change >1.5 and FDR adjusted $p < 0.05$) from a total of 16,563 detected genes between vehicle- and MC-LR–treated follicles, among which 2,028 were up-regulated and 1,340 were down-regulated in MC-LR–treated follicles compared with control follicles. Consistent with the RT-qPCR data, the expression of all follicle maturation-related genes examined in Figure 6 were significantly lower in the RNA-seq analysis of MC-LR–treated follicles (Figure 7B).

DEGs were next used for Gene Ontology (GO) term enrichment and Kyoto Encyclopedia of Genes and Genomes (KEGG)

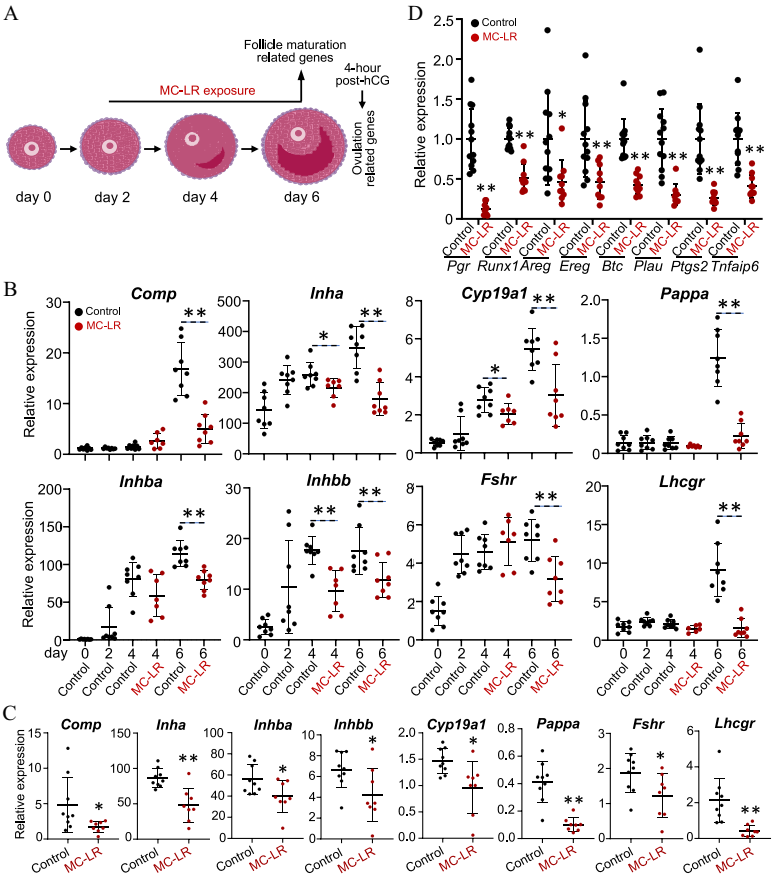

Figure 6. Effects of MC-LR treatment on the expression of follicle maturation and ovulation-related genes *in vitro*. (A) The schematic of MC-LR exposure *in vitro* using eIVFG to investigate the mechanisms of MC-LR on follicle maturation and ovulation. (B) Expression of follicle maturation-related genes in vehicle- and MC-LR treated follicles. $N = 7$–8 follicles in each group. (C) Expression of follicle maturation-related genes in isolated mural granulosa cells from vehicle- and MC-LR–treated follicles. $N = 8$–9 follicles in each group. (D) Expression of established ovulatory genes in vehicle- or MC-LR–treated follicles that were collected at 4 h post-hCG. $N = 10$–12 follicles in each group. The mRNA expression levels of each gene were normalized by the expression of glyceraldehyde-3-phosphate dehydrogenase (*Gapdh*). Data were analyzed with one-way ANOVA followed by a Tukey's multiple comparisons test (B) and Student's *t*-test (C,D). Bidirectional error bars represent mean ± standard deviation; $^{*}p < 0.05$ and $^{**}p < 0.01$. Data in (B–D) are also presented in Tables S22, S23, and S25, respectively. Note: ANOVA, analysis of variance; eIVFG, encapsulated *in vitro* follicle growth; hCG, human chorionic gonadotropin; MC-LR, microcystin-LR.

pathway analyses. Biological process analysis demonstrated that DEGs were primarily enriched in the processes of cell adhesion, angiogenesis, cell migration, inflammatory response, and cell proliferation (Figure 7C; Table S27). Molecular function analysis showed that DEGs were mainly related to the functions of binding of biomolecules, such as protein, heparin, integrin, calcium ion, extracellular matrix, and fibronectin (Figure 7D; Table S28). Cellular component analysis revealed that DEGs were closely related to the components of basement membrane, extracellular matrix, and extracellular exosome (Figure 7E; Table S29). KEGG pathway analysis identified several significantly altered signaling pathways upon MC-LR treatment, such as pathways related to extracellular matrix (ECM)-receptor interaction, focal adhesion, and importantly, PI3K/AKT signaling (Figure 7F; Table S30).

Based on a previous study that discovered numerous FOXO1 target genes in an *in vitro* rat granulosa cell culture model,[55] we found that 315 genes were also significantly altered in follicles treated with MC-LR *in vitro*, including 189 up- and 126 down-regulated genes (Table S31). Among these overlapped 315 genes between the two data sets, many of them critically govern follicular events during follicle maturation, such as ovarian steroidogenesis (*Cyp17a1*, *Hsd17b1*, *Cyp19a1*, and *Nr5a1*), peptide hormone secretion (*Inha*, *Inhba*, and *Inhbb*), IGF-dependent activation of PI3K/AKT signaling (*Pappa*), and oocyte meiotic arrest (*Nppc*) (Figure 7G; Table S32). Moreover, RNA-seq analysis identified many additional genes (Figure 7G) and signaling pathways (Figure 7C-7F), suggesting they may also play critical roles in MC-LR–induced defective follicle maturation.

Impacts of MC-LR on PP1-Mediated Activation of PI3K/AKT/FOXO1 Signaling

PP1 is an essential molecular component mediating the cross-talk between the FSH- and IGF-stimulated signaling pathways that underpin follicle maturation.[36,37] MC-LR has been shown to selectively and covalently bind to the catalytic subunits of PP1 or PP2A to irreversibly inhibit their phosphatase activities,[16,17] which might underlie the MC-LR–induced defect of follicle maturation. To test this hypothesis, we first examined the activities of PP1 and PP2A in follicles treated with vehicle or 10 μM MC-LR from day 2 to day 6 of eIVFG. Protein phosphatase assays showed that the phosphatase activities of PP1 but not PP2A were significantly reduced in MC-LR–treated follicles (Figure 8A,B; Tables S33 and S34). Next, follicles with the same vehicle or MC-LR treatment method were collected on day 6 of eIVFG to examine the intrafollicular accumulation of MC-LR, the phosphorylation status of key proteins contributing to the activation of

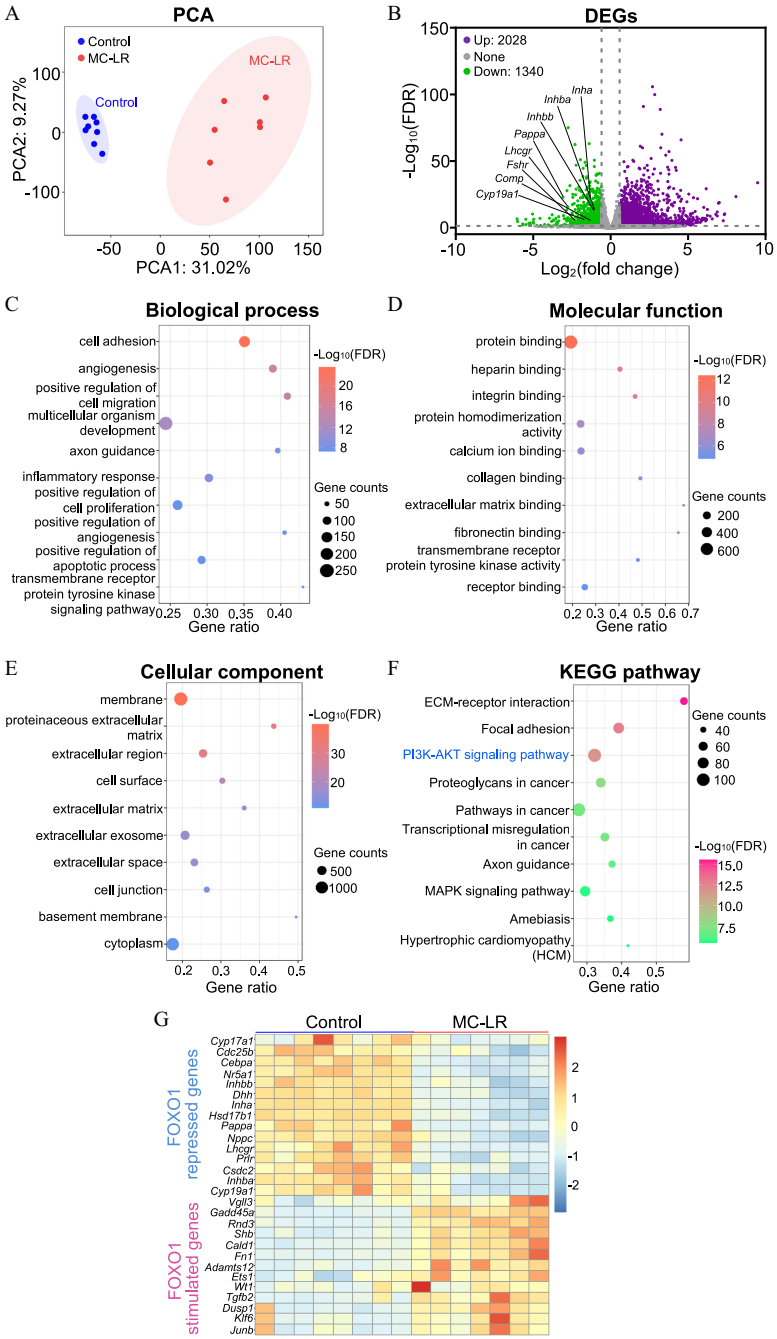

Figure 7. Single-follicle RNA-sequencing analysis of MC-LR–treated follicles *in vitro*. (A) Principal component analysis (PCA) of the first two principal components between vehicle ($N = 8$)- and MC-LR ($N = 7$)-treated follicles. All follicles were located within the 95% confidence interval, represented by the blue (control) and red (MC-LR) ellipses. (B) Volcano plot of differentially expressed genes (DEGs; FDR <0.05, absolute fold change >1.5) in MC-LR–treated follicles compared with the control group. Purple: up-regulated genes; gray: nonsignificantly altered genes; green: down-regulated genes. Gene Ontology (GO) analyses of DEGs, including (C) top 10 biological process enrichment results, (D), top 10 molecular function enrichment results, and (E) top 10 cellular component enrichment results. (F) Top 10 KEGG pathway enrichment results of DEGs. (G) Heatmap of representative overlapped genes between DEGs identified in MC-LR–treated murine follicles and FOXO1 target genes identified in rat granulosa cells. Data in (C–G) are also presented in Tables S27–S30 and S32, respectively. Note: ECM, extracellular matrix; FDR, false discovery rate; KEGG, Kyoto Encyclopedia of Genes and Genomes; MC-LR, microcystin-LR.

the PI3K/AKT/FOXO1 signaling, and biomarkers indicative of follicle growth and survival. Western blotting revealed that MC-LR accumulated in cultured follicles (Figure 8C). Exposure to MC-LR significantly resulted in higher and lower phosphorylation of AKT(Ser^{473}) and AKT(Thr^{308}), respectively (Figure 8C, D; Table S35); the dual phosphorylation modification of these two amino acid residues are indispensable for the activation of AKT.[56] The phosphorylation of FOXO1 was significantly lower in those follicles exposed to MC-LR (Figure 8C,D; Table S35). Western blotting results also revealed that MC-LR exposure did not result in different expression of γH2AX, a DNA damage marker, or PCNA, a cell proliferation marker (Figure 8C,D; Table S35).

To further confirm the causal relationship between the disrupted PI3K/AKT/FOXO1 signaling caused by MC-LR and the defective follicle maturation and ovulation, we co-treated

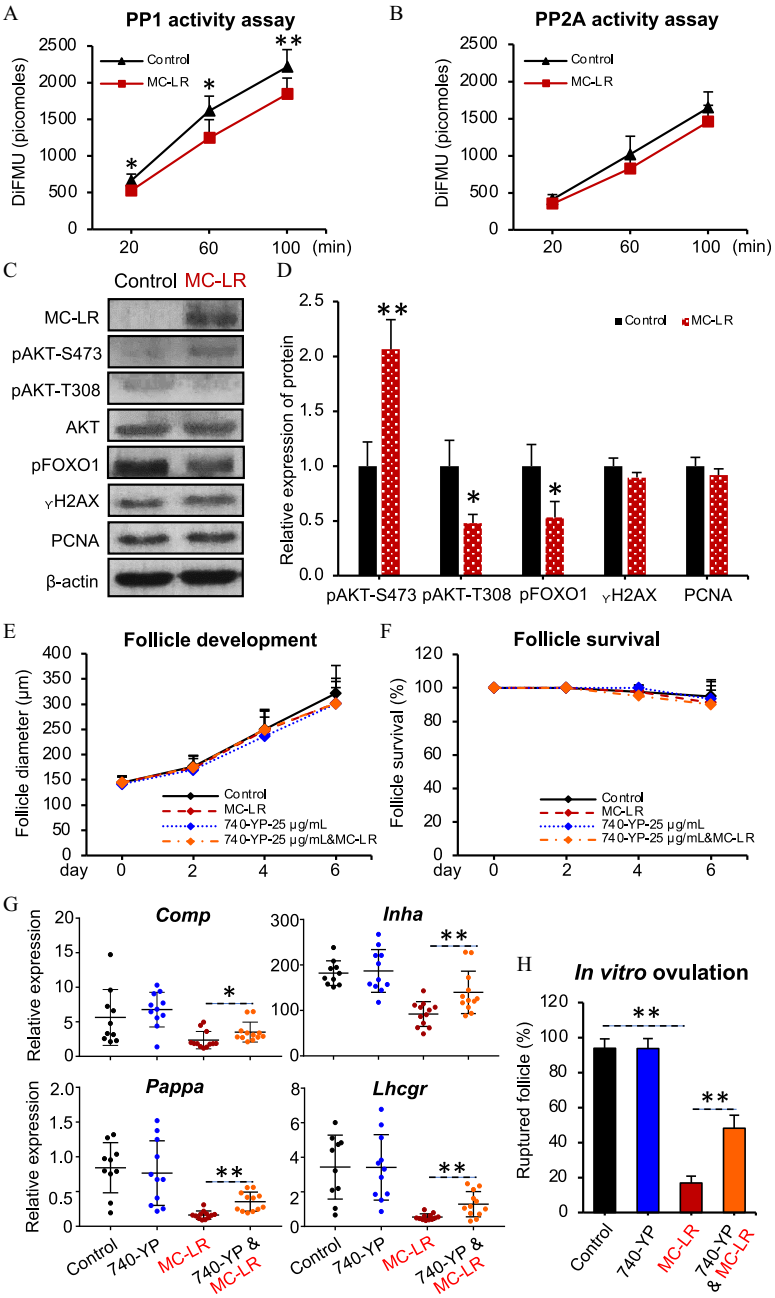

Figure 8. Effects of MC-LR exposure on the PP1-mediated activation of PI3K/AKT/FOXO1 signaling. A time course assessment of (A) PP1 and (B) PP2A phosphatase activities in vehicle- or 10 μM MC-LR–treated follicles on day 6 of eIVFG. $N = 25$–30 follicles in each group, and three independent replicates were included. (C) Western blotting analysis of MC-LR, γH2AX, PCNA, and key regulators of the PI3K/AKT/FOXO1 signaling in follicles treated with vehicle or 10 μM MC-LR. $N = 20$–25 follicles were pooled to obtain sufficient amounts of proteins and three independent replicates were included. (D) Quantification of examined proteins by western blotting. (E) Diameters and (F) survival rates of follicles treated with vehicle or 10 μM MC-LR in the presence or absence of 25 μg/mL 740-YP. $N = 12$–15 follicles in each group per replicate, and three replicates were included. (G) Expression of follicle maturation-related genes in follicles collected from day 6 of eIVFG. Follicles were treated with vehicle, 10 μM MC-LR, 25 μg/mL 740-YP, and co-treatment of 10 μM MC-LR and 25 μg/mL 740-YP from day 2 to day 6 of eIVFG. The mRNA expression levels of each gene were normalized by the expression of glyceraldehyde-3-phosphate dehydrogenase (*Gapdh*). $N = 10$–12 follicles in each group. (H) Percentages of ruptured follicles at 16 h post-hCG with follicles treated with vehicle, 10 μM MC-LR, 25 μg/mL 740-YP, and co-treatment of 10 μM MC-LR and 25 μg/mL 740-YP from day 2 to day 6 of eIVFG. Follicles were treated with 1.5 IU/mL hCG on day 6 of eIVFG for ovulation induction. $N = 10$–12 follicles in each group per replicate, and three replicates were included. Data were analyzed with Student's *t*-test (A,B,D) and one-way ANOVA followed by a Tukey's multiple comparisons test (E–H). Bidirectional error bars represent mean ± standard deviation; $^{*}p < 0.05$ and $^{**}p < 0.01$. Data in (A,B,D–H) are also presented in Tables S33–S39, respectively. Note: ANOVA, analysis of variance; DiFMU, 6,8-difluoro-7-hydroxy-4-methylcoumarin (reference standard); eIVFG, encapsulated *in vitro* follicle growth; hCG, human chorionic gonadotropin; MC-LR, microcystin-LR; PP1, protein phosphatase 1; PP2A, protein phosphatase 2A.

follicles with 10 μM MC-LR and 25 μg/mL 740-YP, a potent PI3K activator.[57] Treatment with 740-YP alone did not affect follicle development, survival, expression of follicle maturation-related genes, and ovulation (Figure 8E–8H; Tables S36–S39). However, the co-treatment of 740-YP significantly reversed the MC-LR–induced reduction of follicle maturation-related genes as well as the inhibited ovulation (Figure 8G–8H; Tables S38 and S39).

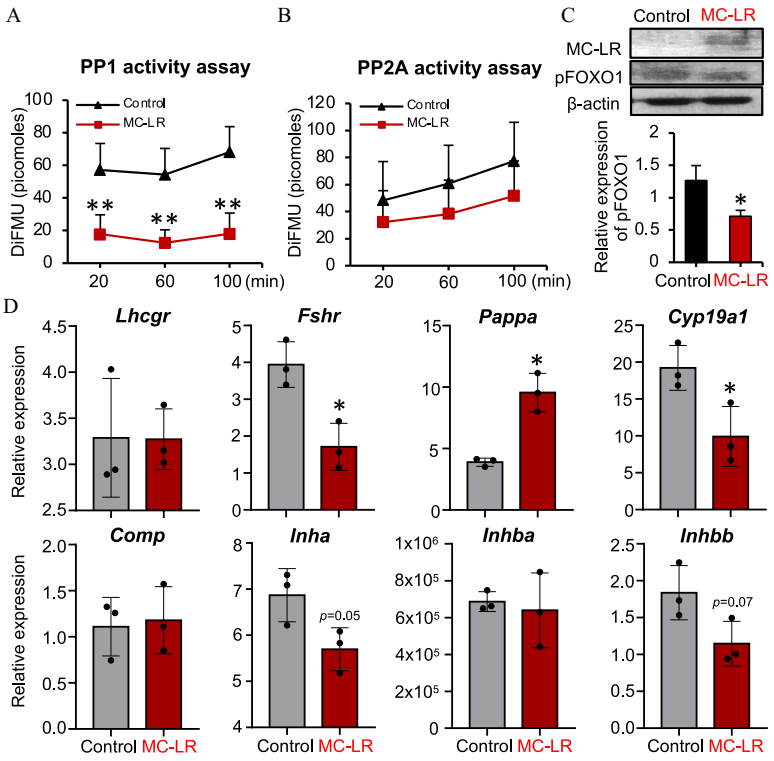

Figure 9. Effects of MC-LR on the PP1-mediated activation of PI3K/AKT/FOXO1 signaling and the expression of follicle maturation-related genes in human primary granulosa cells. A time course assessment of (A) PP1 and (B) PP2A phosphatase activities in vehicle- or 10 μM MC-LR–treated human primary granulosa cells. Three independent replicates included. (C) Western blotting analysis of MC-LR and phosphorylated FOXO1 in human primary granulosa cells treated with vehicle or 10 μM MC-LR. Three independent replicates were included. (D) Expression of follicle maturation-related genes in vehicle- or 10 μM MC-LR–treated human primary granulosa cells. The mRNA expression levels of each gene were normalized by the expression of glyceraldehyde-3-phosphate dehydrogenase (*Gapdh*). Three independent replicates were included. $N = 3$ for each group. Data were analyzed with Student's *t*-test (A–D). Bidirectional error bars represent mean ± standard deviation; $^{*}p < 0.05$ and $^{**}p < 0.01$. Data in (A–D) are also presented in Tables S40–S43, respectively. Note: DiFMU, 6,8-difluoro-7-hydroxy-4-methylcoumarin (reference standard); MC-LR, microcystin-LR; PP1, protein phosphatase 1; PP2A, protein phosphatase 2A.

Effects of MC-LR Exposure on Human Primary Granulosa Cells

To investigate whether MC-LR induces similar ovarian toxicities in humans, we treated human primary luteinizing granulosa cells with vehicle or 10 μM MC-LR for 24 h *in vitro* and examined the phosphatase activities of PP1 and PP2A, the activation of PI3K/AKT/FOXO1 signaling, and the expression of follicle maturation-related genes. Consistent with results from both *in vivo* and *in vitro* murine models, cells exposed to MC-LR had significantly lower phosphatase activities of PP1 but not PP2A (Figure 9A,B; Tables S40 and S41). Western blotting results showed that MC-LR accumulated in human granulosa cells, and cells exposed to MC-LR had significantly reduced phosphorylation of FOXO1 (Figure 9C; Table S42). In addition, cells exposed to MC-LR had significantly lower expression of several follicle maturation-related genes, including *Fshr*, *Cyp19a1*, *Inha*, and *Inhbb* (Figure 9D; Table S43). Intriguingly, cells exposed to MC-LR had similar expression of *Lhcgr*, *Comp*, and *Inhba,* and even higher expression of *Pappa* compared with control cells (Figure 9D; Table S43).

Discussion

Substantial increases of CyanoHABs have made CyanoHAB toxins global contaminants of emerging concern.[58] So far, the impact of CyanoHAB toxins on women's reproductive health remains poorly explored. Here, results in both *in vivo* mouse exposure models and *in vitro* cultures of murine ovarian follicles and human primary granulosa cells suggest that MC-LR at environmentally relevant exposure levels interfered with PP1-mediated PI3K/AKT/FOXO1 signaling in follicular granulosa cells, which disrupted FSH-dependent follicle maturation and resulted in defective ovulation, luteinization, progesterone secretion, and other female reproductive outcomes.

Although a range of stakeholders are aware of the emerging CyanoHAB toxins, including MCs, these toxins are not routinely monitored due to the absence of federal/state regulatory guidelines, and the conventional water treatments also cannot completely remove dissolved CyanoHAB toxins.[59] Because of the high physiochemical stability of CyanoHAB toxins, boiling or microwaving drinking water may even increase the release of toxins from the lyses of cyanobacterial cells and evaporation.[60] The incidental swollen of contaminated water during swimming would be additional potential exposure to high concentration of MC-LR during cyanobacterial blooming seasons. Moreover, the contamination levels of CyanoHAB toxins can be >10–10,000 folds higher than the WHO/U.S. EPA drinking water health advisories during peak bloom seasons.[61] For instance, the 95th percentile of the total MC toxin concentration detected in New Jersey lakes was reported to be 4.38 μg/L, with the highest level reached 1,096.5 μg/L during the past 4 y (2017–2020).[41] In this study, we treated young adult female mice with 10 μg/kg per day MC-LR by daily oral gavage for 6 wk, which is close to or even lower than the NOAELs (17–40 μg/kg per day) for liver toxicities observed in rodents that were used as the basis of drinking water guidance values developed by the U.S. EPA[41] and the WHO.[42]

The human serum concentrations of MC-LR have been found to be at 0.05–1.8 nM in fishermen in Lake Chaohu, China,[62] and 7.6–31.4 nM in patients treated with MC-LR–contaminated dialysate

fluids in Caruaru, Brazil.[63] Using the 3D *in vitro* follicle culture model, we found that the $BMCL_{10}$ of MC-LR was 0.38 μM and 0.14 μM for failed follicle rupture and completion of oocyte meiosis I during *in vitro* ovulation, respectively. Using an uncertainty factor of 100 for *in vitro* to *in vivo* extrapolation, these $BMCL_{10}$ values will translate to 1.4–3.7 nM as reference concentrations for 10% extra risk of ovulation defects. Given the serum concentration ranges in humans listed above, it is reasonable to argue that for high-exposure populations, such as fisherman and people with accidental exposure to CyanoHAB toxins, particularly the MC-LR, the margin of safety is small, and there may be some nonnegligible risk for women's reproductive health.

There are several possibilities to explain the lower CL number in the long-term low-dose oral exposure to MC-LR experiment, involving MC-LR–mediated perturbations of preovulatory, ovulatory, or postovulatory events: *a*) MC-LR may disrupt the molecular events intrinsic to the ovulation process per se such that terminally mature follicles fail to ovulate and differentiate into CL; *b*) although antral follicles appear morphologically normal under MC-LR exposure, there could be molecular alterations during follicle maturation that disrupt the readiness of the seemingly mature antral follicles for responding to the ovulatory LH surge; and *c*) MC-LR may disrupt the luteinization of postovulatory follicular cells to form CL and/or promote the apoptosis of CL cells. Using both *in vivo* mouse superovulation models involving three different MC-LR exposure windows and *in vitro* follicle culture model, our results suggest that MC-LR may have caused an aberration in follicle maturation, which further resulted in a secondary disruption on the follicle ovulation and the formation of CL.

Based on our *in vivo* exposure results, the defective follicle maturation and ovulation may have been due to the direct effects of MC-LR on the ovary but not the secretion of gonadotropins. The direct ovarian impact of MC-LR was further confirmed by *in vitro* exposure experiments using both murine follicles and human granulosa cells, suggesting that MC-LR significantly inhibited FSH/PP1-stimulated PI3K/AKT/FOXO1 signaling and downstream FSH target genes. For instance, expression of both PAPPA and LHCGR were markedly lower in granulosa cells of MC-LR–treated follicles *in vivo* and *in vitro*. PAPPA functions to cleave IGF binding proteins and release bioactive IGF to potentiate the activation of the PI3K/AKT/FOXO1 pathway in granulosa cells during follicle maturation.[64–66] It is highly likely that the reduction of PAPPA under MC-LR exposure lessened the release of bioactive IGF, which led to inadequate activation of PI3K/AKT/FOXO1 signaling and induction of FSH target genes. The induction of LHCGR in granulosa cells enables maturing follicles to eventually become responsive to the LH surge for ovulation.[67] Thus, in MC-LR–treated follicles, the lower expression of LHCGR in granulosa cells could desensitize antral follicles to LH or hCG, leading to ovulation failure. Indeed, the failed ovulation resulting from the suppression of LHCGR was further confirmed by the lower expression of LH-target genes (e.g., *Pgr*, *Runx1*, *Areg*, *Ereg*, and *Btc*) at 4 h post-hCG in follicles treated with MC-LR.

A previous study from Herndon et al. identified 2,264 FOXO1 target genes in rat granulosa cells.[55] Our single-follicle RNA-seq data showed that 315 (13.9% of DEGs) FOXO1 target genes identified by Herndon et al. were consistently up- or down-regulated by MC-LR in this study, including several established follicle maturation-related genes listed in Table S12 (e.g., *Cyp19a1*, *Pappa*, and *Lhcgr*). Regarding those nonoverlapped genes, there are several possibilities. First, in addition to activating PI3K/AKT/FOXO1 signaling, FSH also stimulates other pathways during follicle maturation, including CREB,[68] EGFR,[69] ERK,[70] and p38 MAPK,[71] which may also serve as targets of MC-LR. Second, Herndon et al. used rat granulosa cells, but our RNA-seq analysis

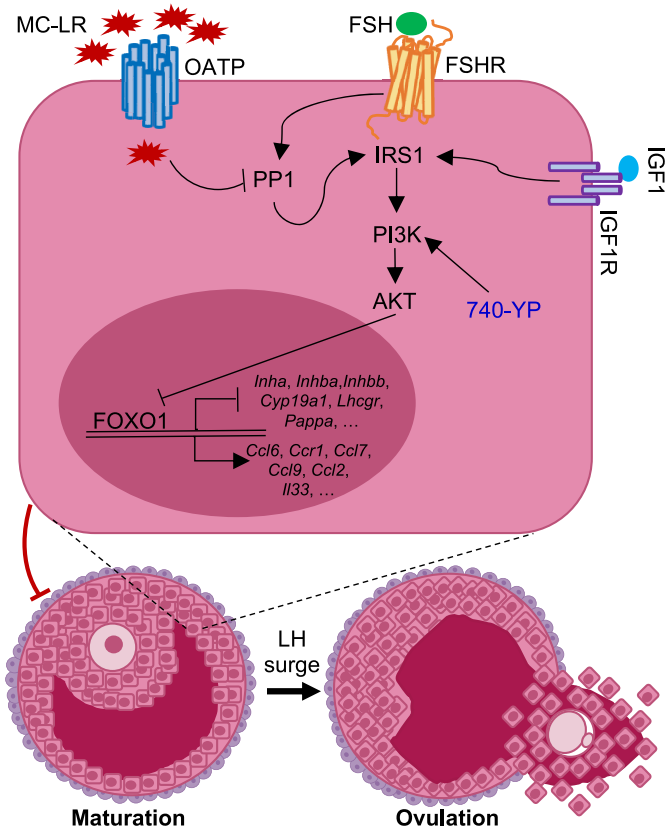

Figure 10. The proposed molecular mechanism by which MC-LR interferes with PP1-mediated PI3K/AKT/FOXO1 signaling in follicular granulosa cells to disrupt gonadotropin-dependent follicle maturation and ovulation. Note: 740-YP, a potent PI3K activator; AKT, serine/threonine kinase 1; FSH, follicle-stimulating hormone; FSHR, follicle-stimulating hormone receptor; IGF1, insulin-like growth factor 1; IGF1R, insulin-like growth factor 1 receptor; IRS1, insulin receptor substrate 1; LH, luteinizing hormone; MC-LR, microcystin-LR; OATP, organic anion transporting polypeptide (shown to regulate the cellular uptake of MC-LR); PI3K, phosphatidylinositol 3-kinase; PP1, protein phosphatase 1.

was based on single mouse follicles. Thus, the species difference and/or the more inclusive follicular cell types (theca cells, granulosa cells, and oocyte) in our study may have generated different sets of DEGs. Last, the nonoverlapping DEGs might be due to toxic mechanisms independent of PP1 and PI3K/AKT/FOXO1 signaling. For instance, our single-follicle RNA-seq results showed that the expression of several oxidative stress-related genes (27 among 91 examined genes) was significantly different in MC-LR–treated follicles compared with control (Table S44). In addition, there were two genes, *Atg4c* and *Gabarapl1*, that were significantly down- and up-regulated, respectively, in MC-LR–treated follicles among 34 established autophagy-related genes (Table S45). Furthermore, MC-LR increased the follicular expression of several inflammatory genes, such as *Ccl6*, *Ccr1*, *Ccl7*, *Ccl9*, *Ccl2*, and *Il33* (Table S46). The aberrant inflammatory response in the ovary has been associated with polycystic ovary syndrome (PCOS) and reproductive aging, both of which also exhibit defective follicle maturation and ovulation.[72] In addition, PI3K activator 740-YP could not completely rescue the MC-LR–induced reduction of follicle maturation genes and the inhibited ovulation, implying that other mechanisms were also included in MC-LR–compromised follicle maturation and ovulation. Therefore, oxidative stress, autophagy, and inflammation may also contribute to the MC-LR–induced defects in follicle maturation, but their specific roles in this regard require more in-depth investigations in future studies.

Meanwhile, more selective PP1 activators and inhibitors can be used to further confirm the causal relationship between MC-LR–induced PP1 inhibition and defective activation of PP1-meidated PI3K/AKT/FOXO1 signaling pathway during gonadotropin-dependent follicle maturation and ovulation.

In addition to PP1, MC-LR also inhibits the phosphatase activity of PP2A through a similar mechanism.[16,17] However, we found that both murine and human granulosa cells exposed to MC-LR did not have different phosphatase activities of PP2A compared with control cells. It has been reported that although there were more ovulated eggs with aneuploidy in mice lacking PP2A, they had normal follicle development and preovulatory follicles were responsive to the LH surge to undergo ovulation.[73,74] These results suggest a dispensable role of PP2A in folliculogenesis, and the unchanged phosphatase activity of PP2A in MC-LR–treated follicles and granulosa cells indicates that PP2A may remain at a basal level in granulosa cells during FSH-dependent follicle maturation.

In conclusion, as depicted in Figure 10, our study supports the idea that MC-LR acts as a selective PP1 inhibitor to interfere with PP1-mediated PI3K/AKT/FOXO1 signaling in granulosa cells, disrupting FSH-dependent follicle maturation and associated female reproductive outcomes. As a new endocrine disrupting chemical and reproductive toxicant, exposure to MC-LR, particularly during CyanoHAB bloom seasons, may heighten women's risk of ovarian disorders associated with FSH-dependent follicle maturation, including anovulation, irregular menstrual cycles, infertility, and also the common ovarian diseases of PCOS and luteinized unruptured follicle syndrome. In the future, both human-based epidemiological studies and research models using more representative human ovarian samples (e.g., *in vitro* culture of human follicles or primary granulosa cells from human early antral follicles) are required to confirm this hypothesis.

Acknowledgments

Y.W. contributed to the experimental design, data collection and analysis, and manuscript writing. P.P., J.Z., E.K., E.A.J., and D.Z. contributed to the data collection and analysis. M.F., Y.Y., S.C., J-Y.J.K, and G.I.S. contributed to the data interpretation and manuscript writing. Q.Z. contributed to the experimental design, data analysis, and manuscript writing. S.X. conceived of the project, designed experiments, collected, analyzed, and interpreted data, wrote the manuscript, and provided final approval of the manuscript.

This work was supported by the National Institutes of Health (NIH) K01ES030014 and P30ES005022 to S.X., R01ES032144 to S.X. and Q.Z., P01ES028942 to G.I.S., S.C., and S.X., UH3ES029073 to J.K. and S.X. and by the startup fund from the Environmental and Occupational Health Sciences Institute at Rutgers University to S.X. The manuscript has been subjected to review by the New Jersey Department of Environmental Protection (NJDEP) Division and Science and Research and approved for publication, but the views expressed do not necessarily reflect the views or policy of the NJDEP.

References

1. Brooks BW, Lazorchak JM, Howard MDA, Johnson MVV, Morton SL, Perkins DAK, et al. 2016. Are harmful algal blooms becoming the greatest inland water quality threat to public health and aquatic ecosystems? Environ Toxicol Chem 35(1):6–13, PMID: 26771345, https://doi.org/10.1002/etc.3220.
2. Landrigan PJ, Stegeman JJ, Fleming LE, Allemand D, Anderson DM, Backer LC, et al. 2020. Human health and ocean pollution. Ann Glob Health 86(1):151, PMID: 33354517, https://doi.org/10.5334/aogh.2831.
3. Pham TL, Utsumi M. 2018. An overview of the accumulation of microcystins in aquatic ecosystems. J Environ Manage 213:520–529, PMID: 29472035, https://doi.org/10.1016/j.jenvman.2018.01.077.
4. Bouaïcha N, Miles CO, Beach DG, Labidi Z, Djabri A, Benayache NY, et al. 2019. Structural diversity, characterization and toxicology of microcystins. Toxins (Basel) 11(12):714, PMID: 31817927, https://doi.org/10.3390/toxins11120714.
5. Tsuji K, Watanuki T, Kondo F, Watanabe MF, Suzuki S, Nakazawa H, et al. 1995. Stability of microcystins from cyanobacteria—II. Effect of UV light on decomposition and isomerization. Toxicon 33(12):1619–1631, PMID: 8866619, https://doi.org/10.1016/0041-0101(95)00101-8.
6. Drobac D, Tokodi N, Simeunović J, Baltić V, Stanić D, Svirčev Z. 2013. Human exposure to cyanotoxins and their effects on health. Arh Hig Rada Toksikol 64(2):119–130, PMID: 23819940, https://doi.org/10.2478/10004-1254-64-2013-2320.
7. Vidal F, Sedan D, D'Agostino D, Cavalieri ML, Mullen E, Parot Varela M, et al. 2017. Recreational exposure during algal bloom in Carrasco Beach, Uruguay: a liver failure case report. Toxins (Basel) 9(9):267, PMID: 28858213, https://doi.org/10.3390/toxins9090267.
8. Wijewickrama MM, Manage PM. 2019. Accumulation of microcystin-LR in grains of two rice varieties (*Oryza sativa L.*) and a leafy vegetable, *Ipomoea aquatica*. Toxins (Basel) 11(8):432, PMID: 31344839, https://doi.org/10.3390/toxins11080432.
9. Pouria S, de Andrade A, Barbosa J, Cavalcanti RL, Barreto VT, Ward CJ, et al. 1998. Fatal microcystin intoxication in haemodialysis unit in Caruaru, Brazil. Lancet 352(9121):21–26, PMID: 9800741, https://doi.org/10.1016/s0140-6736(97)12285-1.
10. Miura GA, Robinson NA, Lawrence WB, Pace JG. 1991. Hepatotoxicity of microcystin-LR in fed and fasted rats. Toxicon 29(3):337–346, PMID: 2048148, https://doi.org/10.1016/0041-0101(91)90287-2.
11. Hinojosa MG, Gutiérrez-Praena D, Prieto AI, Guzmán-Guillén R, Jos A, Cameán AM. 2019. Neurotoxicity induced by microcystins and cylindrospermopsin: a review. Sci Total Environ 668:547–565, PMID: 30856566, https://doi.org/10.1016/j.scitotenv.2019.02.426.
12. Svircev Z, Baltić V, Gantar M, Juković M, Stojanović D, Baltić M. 2010. Molecular aspects of microcystin-induced hepatotoxicity and hepatocarcinogenesis. J Environ Sci Health C Environ Carcinog Ecotoxicol Rev 28(1):39–59, PMID: 20390967, https://doi.org/10.1080/10590500903585382.
13. Arman T, Clarke JD. 2021. Microcystin toxicokinetics, molecular toxicology, and pathophysiology in preclinical rodent models and humans. Toxins (Basel) 13(8):537, PMID: 34437407, https://doi.org/10.3390/toxins13080537.
14. McLellan NL, Manderville RA. 2017. Toxic mechanisms of microcystins in mammals. Toxicol Res (Camb) 6(4):391–405, PMID: 30090507, https://doi.org/10.1039/c7tx00043j.
15. Chen L, Chen J, Zhang X, Xie P. 2016. A review of reproductive toxicity of microcystins. J Hazard Mater 301:381–399, PMID: 26521084, https://doi.org/10.1016/j.jhazmat.2015.08.041.
16. MacKintosh C, Beattie KA, Klumpp S, Cohen P, Codd GA. 1990. Cyanobacterial microcystin-LR is a potent and specific inhibitor of protein phosphatase-1 and phosphatase-2A from both mammals and higher plants. FEBS Lett 264(2):187–192, PMID: 2162782, https://doi.org/10.1016/0014-5793(90)80245-e.
17. Xing Y, Xu Y, Chen Y, Jeffrey PD, Chao Y, Lin Z, et al. 2006. Structure of protein phosphatase 2A core enzyme bound to tumor-inducing toxins. Cell 127(2):341–353, PMID: 17055435, https://doi.org/10.1016/j.cell.2006.09.025.
18. Ramos F, Villoria MT, Alonso-Rodríguez E, Clemente-Blanco A. 2019. Role of protein phosphatases PP1, PP2A, PP4 and Cdc14 in the DNA damage response. Cell Stress 3(3):70–85, PMID: 31225502, https://doi.org/10.15698/cst2019.03.178.
19. Wlodarchak N, Xing YN. 2016. PP2A as a master regulator of the cell cycle. Crit Rev Biochem Mol Biol 51(3):162–184, PMID: 26906453, https://doi.org/10.3109/10409238.2016.1143913.
20. Shi Y, Reddy B, Manley JL. 2006. PP1/PP2A phosphatases are required for the second step of pre-mRNA splicing and target specific snRNP proteins. Mol Cell 23(6):819–829, PMID: 16973434, https://doi.org/10.1016/j.molcel.2006.07.022.
21. Campos A, Vasconcelos V. 2010. Molecular mechanisms of microcystin toxicity in animal cells. Int J Mol Sci 11(1):268–287, PMID: 20162015, https://doi.org/10.3390/ijms11010268.
22. Žegura B, Štraser A, Filipič M. 2011. Genotoxicity and potential carcinogenicity of cyanobacterial toxins—a review. Mutat Res 727(1–2):16–41, PMID: 21277993, https://doi.org/10.1016/j.mrrev.2011.01.002.
23. Mallia V, Ivanova L, Eriksen GS, Harper E, Connolly L, Uhlig S. 2020. Investigation of *in vitro* endocrine activities of *Microcystis* and *Planktothrix* cyanobacterial strains. Toxins (Basel) 12(4):228, PMID: 32260386, https://doi.org/10.3390/toxins12040228.
24. Rogers ED, Henry TB, Twiner MJ, Gouffon JS, McPherson JT, Boyer GL, et al. 2011. Global gene expression profiling in larval zebrafish exposed to microcystin-LR and *Microcystis* reveals endocrine disrupting effects of Cyanobacteria. Environ Sci Technol 45(5):1962–1969, PMID: 21280650, https://doi.org/10.1021/es103538b.
25. Wu J, Shao S, Zhou F, Wen S, Chen F, Han X. 2014. Reproductive toxicity on female mice induced by microcystin-LR. Environ Toxicol Pharmacol 37(1):1–6, PMID: 24280256, https://doi.org/10.1016/j.etap.2013.10.012.
26. Wu J, Yuan M, Song Y, Sun F, Han X. 2015. MC-LR exposure leads to subfertility of female mice and induces oxidative stress in granulosa cells. Toxins (Basel) 7(12):5212–5223, PMID: 26633508, https://doi.org/10.3390/toxins7124872.

27. Zhan C, Zhang F, Liu W, Zhang X. 2020. Microcystin-LR promotes zebrafish (*Danio rerio*) oocyte (*in vivo*) maturation by activating ERK1/2-MPF signaling pathways, and cAMP is involved in this process. Environ Pollut 259:113843, PMID: 31887595, https://doi.org/10.1016/j.envpol.2019.113843.
28. Trinchet I, Djediat C, Huet H, Dao SP, Edery M. 2011. Pathological modifications following sub-chronic exposure of medaka fish (*Oryzias latipes*) to microcystin-LR. Reprod Toxicol 32(3):329–340, PMID: 21839164, https://doi.org/10.1016/j.reprotox.2011.07.006.
29. Du X, Liu H, Liu X, Chen X, Yuan L, Ma Y, et al. 2021. Microcystin-LR induces ovarian injury and apoptosis in mice via activating apoptosis signal-regulating kinase 1-mediated P38/JNK pathway. Ecotoxicol Environ Saf 213:112066, PMID: 33610944, https://doi.org/10.1016/j.ecoenv.2021.112066.
30. Liu H, Tian Z, Guo Y, Liu X, Ma Y, Du X, et al. 2021. Microcystin-leucine arginine exposure contributes to apoptosis and follicular atresia in mice ovaries by endoplasmic reticulum stress-upregulated Ddit3. Sci Total Environ 756:144070, PMID: 33288253, https://doi.org/10.1016/j.scitotenv.2020.144070.
31. Ma Y, Liu H, Du X, Petlulu P, Chen X, Wang R, et al. 2021. IRE1 and CaMKKβ pathways to reveal the mechanism involved in microcystin-LR-induced autophagy in mouse ovarian cells. Food Chem Toxicol 147:111911, PMID: 33290805, https://doi.org/10.1016/j.fct.2020.111911.
32. Zhang X, Zhou C, Li W, Li J, Wu W, Tao J, et al. 2020. Vitamin C protects porcine oocytes from microcystin-LR toxicity during maturation. Front Cell Dev Biol 8:582715, PMID: 33134299, https://doi.org/10.3389/fcell.2020.582715.
33. Edson MA, Nagaraja AK, Matzuk MM. 2009. The mammalian ovary from genesis to revelation. Endocr Rev 30(6):624–712, PMID: 19776209, https://doi.org/10.1210/er.2009-0012.
34. Dierich A, Sairam MR, Monaco L, Fimia GM, Gansmuller A, LeMeur M, et al. 1998. Impairing follicle-stimulating hormone (FSH) signaling *in vivo:* targeted disruption of the FSH receptor leads to aberrant gametogenesis and hormonal imbalance. Proc Natl Acad Sci U S A 95(23):13612–13617, PMID: 9811848, https://doi.org/10.1073/pnas.95.23.13612.
35. Casarini L, Crépieux P. 2019. Molecular mechanisms of action of FSH. Front Endocrinol (Lausanne) 10:305, PMID: 31139153, https://doi.org/10.3389/fendo.2019.00305.
36. Law NC, Hunzicker-Dunn ME. 2016. Insulin receptor substrate 1, the hub linking follicle-stimulating hormone to phosphatidylinositol 3-kinase activation. J Biol Chem 291(9):4547–4560, PMID: 26702053, https://doi.org/10.1074/jbc.M115.698761.
37. Law NC, White MF, Hunzicker-Dunn ME. 2016. G protein-coupled receptors (GPCRs) that signal via protein kinase A (PKA) cross-talk at insulin receptor substrate 1 (IRS1) to activate the phosphatidylinositol 3-kinase (PI3K)/AKT pathway. J Biol Chem 291(53):27160–27169, PMID: 27856640, https://doi.org/10.1074/jbc.M116.763235.
38. National Research Council. 2011. *Guide for the Care and Use of Laboratory Animals: Eighth Edition.* Washington, DC: National Academies Press. https://olaw.nih.gov/sites/default/files/Guide-for-the-Care-and-Use-of-Laboratory-Animals.pdf [accessed 2 October 2019].
39. Heinze R. 1999. Toxicity of the cyanobacterial toxin microcystin-LR to rats after 28 days intake with the drinking water. Environ Toxicol 14(1):57–60, https://doi.org/10.1002/(SICI)1522-7278(199902)14:1<57::AID-TOX9>3.0.CO;2-J.
40. Fawell JK, Mitchell RE, Everett DJ, Hill RE. 1999. The toxicity of cyanobacterial toxins in the mouse: I microcystin-LR. Hum Exp Toxicol 18(3):162–167, PMID: 10215106, https://doi.org/10.1177/096032719901800305.
41. U.S. EPA (U.S. Environmental Protection Agency). 2021. Drinking Water Health Advisory Documents for Cyanobacterial Toxins. https://www.epa.gov/ground-water-and-drinking-water/drinking-water-health-advisory-documents-cyanobacterial-toxins [accessed 1 May 2022].
42. WHO (World Health Organization). 2020. *Cyanobacterial toxins: microcystins.* https://apps.who.int/iris/handle/10665/338066 [accessed 15 January 2022].
43. NJDEP (New Jersey Department of Environmental Protection). 2021. Recreational Response Strategy and Annual Summary Reports. https://www.state.nj.us/dep/wms/bfbm/response_strategy.html [accessed 10 January 2022].
44. Lin H, Liu W, Zeng H, Pu C, Zhang R, Qiu Z, et al. 2016. Determination of environmental exposure to microcystin and aflatoxin as a risk for renal function based on 5493 rural people in southwest China. Environ Sci Technol 50(10):5346–5356, PMID: 27071036, https://doi.org/10.1021/acs.est.6b01062.
45. U.S. EPA. 2011. *Exposure Factors Handbook (2011 Edition).* Washington, DC: U.S. EPA. https://www.epa.gov/expobox/exposure-factors-handbook-2011-edition [accessed 20 May 2019].
46. NJDEP. 2021. *Cyanobacterial Harmful Algal Bloom (HAB) Freshwater Recreational Response Strategy.* https://www.state.nj.us/dep/hab/download/HAB2021StrategyFinal.pdf [accessed 20 January 2022].
47. Wang Y, Liu M, Johnson SB, Yuan G, Arriba AK, Zubizarreta ME, et al. 2019. Doxorubicin obliterates mouse ovarian reserve through both primordial follicle atresia and overactivation. Toxicol Appl Pharmacol 381:114714, PMID: 31437492, https://doi.org/10.1016/j.taap.2019.114714.
48. Pedersen T, Peters H. 1968. Proposal for a classification of oocytes and follicles in the mouse ovary. J Reprod Fertil 17(3):555–557, PMID: 5715685, https://doi.org/10.1530/jrf.0.0170555.
49. Schneider CA, Rasband WS, Eliceiri KW. 2012. NIH Image to ImageJ: 25 years of image analysis. Nat Methods 9(7):671–675, PMID: 22930834, https://doi.org/10.1038/nmeth.2089.
50. Crowe AR, Yue W. 2019. Semi-quantitative determination of protein expression using immunohistochemistry staining and analysis: an integrated protocol. Bio Protoc 9(24):e3465, PMID: 31867411, https://doi.org/10.21769/BioProtoc.3465.
51. Wang Y, Xu J, Stanley JE, Xu M, Brooks BW, Scott GI, et al. 2020. A closed vitrification system enables a murine ovarian follicle bank for high-throughput ovotoxicity screening, which identifies endocrine disrupting activity of microcystins. Reprod Toxicol 93:118–130, PMID: 32017985, https://doi.org/10.1016/j.reprotox.2020.01.009.
52. Wang Y, Liu M, Zhang J, Liu Y, Kopp M, Zheng W, et al. 2018. Multidrug resistance protein 1 deficiency promotes doxorubicin-induced ovarian toxicity in female mice. Toxicol Sci 163(1):279–292, PMID: 29462422, https://doi.org/10.1093/toxsci/kfy038.
53. U.S. EPA. 2012. *Benchmark Dose Technical Guidance.* EPA/100/R-12/001. Washington, DC: Risk Assessment Forum, U.S. Environmental Protection Agency. https://www.epa.gov/sites/production/files/2015-01/documents/benchmark_dose_guidance.pdf [accessed 18 April 2022].
54. Fan HY, Liu Z, Shimada M, Sterneck E, Johnson PF, Hedrick SM, et al. 2009. MAPK3/1 (ERK1/2) in ovarian granulosa cells are essential for female fertility. Science 324(5929):938–941, PMID: 19443782, https://doi.org/10.1126/science.1171396.
55. Herndon MK, Law NC, Donaubauer EM, Kyriss B, Hunzicker-Dunn M. 2016. Forkhead box O member FOXO1 regulates the majority of follicle-stimulating hormone responsive genes in ovarian granulosa cells. Mol Cell Endocrinol 434:116–126, PMID: 27328024, https://doi.org/10.1016/j.mce.2016.06.020.
56. Vanhaesebroeck B, Alessi DR. 2000. The PI3K-PDK1 connection: more than just a road to PKB. Biochem J 346(pt 3):561–576, PMID: 10698680, https://doi.org/10.1042/0264-6021:3460561.
57. Li J, Kawamura K, Cheng Y, Liu S, Klein C, Liu S, et al. 2010. Activation of dormant ovarian follicles to generate mature eggs. Proc Natl Acad Sci U S A 107(22):10280–10284, PMID: 20479243, https://doi.org/10.1073/pnas.1001198107.
58. Ho JC, Michalak AM, Pahlevan N. 2019. Widespread global increase in intense lake phytoplankton blooms since the 1980s. Nature 574(7780):667–670, PMID: 31610543, https://doi.org/10.1038/s41586-019-1648-7.
59. Abbas T, Kajjumba GW, Ejjada M, Masrura SU, Marti EJ, Khan E, et al. 2020. Recent advancements in the removal of cyanotoxins from water using conventional and modified adsorbents—a contemporary review. Water 12(10):2756, https://doi.org/10.3390/w12102756.
60. U.S. EPA. 2020. Cyanotoxin Management Tools for Public Water Systems. https://www.epa.gov/ground-water-and-drinking-water/cyanotoxin-management-tools-public-water-systems [accessed 20 January 2022].
61. Welker M, Steinberg C. 1999. Indirect photolysis of cyanotoxins: one possible mechanism for their low persistence. Water Res 33(5):1159–1164, https://doi.org/10.1016/S0043-1354(98)00318-2.
62. Chen J, Xie P, Li L, Xu J. 2009. First identification of the hepatotoxic microcystins in the serum of a chronically exposed human population together with indication of hepatocellular damage. Toxicol Sci 108(1):81–89, PMID: 19151163, https://doi.org/10.1093/toxsci/kfp009.
63. Hilborn ED, Carmichael WW, Yuan M, Azevedo SMFO. 2005. A simple colorimetric method to detect biological evidence of human exposure to microcystins. Toxicon 46(2):218–221, PMID: 15963544, https://doi.org/10.1016/j.toxicon.2005.04.009.
64. Oxvig C. 2015. The role of PAPP-A in the IGF system: location, location, location. J Cell Commun Signal 9(2):177–187, PMID: 25617049, https://doi.org/10.1007/s12079-015-0259-9.
65. Zhou P, Baumgarten SC, Wu Y, Bennett J, Winston N, Hirshfeld-Cytron J, et al. 2013. IGF-I signaling is essential for FSH stimulation of AKT and steroidogenic genes in granulosa cells. Mol Endocrinol 27(3):511–523, PMID: 23340251, https://doi.org/10.1210/me.2012-1307.
66. Nyegaard M, Overgaard MT, Su YQ, Hamilton AE, Kwintkiewicz J, Hsieh M, et al. 2010. Lack of functional pregnancy-associated plasma protein-A (PAPPA) compromises mouse ovarian steroidogenesis and female fertility. Biol Reprod 82(6):1129–1138, PMID: 20130263, https://doi.org/10.1095/biolreprod.109.079517.
67. Pakarainen T, Zhang FP, Nurmi L, Poutanen M, Huhtaniemi I. 2005. Knockout of luteinizing hormone receptor abolishes the effects of follicle-stimulating hormone on preovulatory maturation and ovulation of mouse Graafian follicles. Mol Endocrinol 19(10):2591–2602, PMID: 15941853, https://doi.org/10.1210/me.2005-0075.
68. Salvador LM, Park Y, Cottom J, Maizels ET, Jones JC, Schillace RV, et al. 2001. Follicle-stimulating hormone stimulates protein kinase A-mediated histone H3 phosphorylation and acetylation leading to select gene activation in ovarian granulosa cells. J Biol Chem 276(43):40146–40155, PMID: 11498542, https://doi.org/10.1074/jbc.M106710200.

69. El-Hayek S, Demeestere I, Clarke HJ. 2014. Follicle-stimulating hormone regulates expression and activity of epidermal growth factor receptor in the murine ovarian follicle. Proc Natl Acad Sci USA 111(47):16778–16783, PMID: 25385589, https://doi.org/10.1073/pnas.1414648111.
70. Cottom J, Salvador LM, Maizels ET, Reierstad S, Park Y, Carr DW, et al. 2003. Follicle-stimulating hormone activates extracellular signal-regulated kinase but not extracellular signal-regulated kinase kinase through a 100-kDa phosphotyrosine phosphatase. J Biol Chem 278(9):7167–7179, PMID: 12493768, https://doi.org/10.1074/jbc.M203901200.
71. Maizels ET, Cottom J, Jones JC, Hunzicker-Dunn M. 1998. Follicle stimulating hormone (FSH) activates the p38 mitogen-activated protein kinase pathway, inducing small heat shock protein phosphorylation and cell rounding in immature rat ovarian granulosa cells. Endocrinology 139(7):3353–3356, PMID: 9645711, https://doi.org/10.1210/endo.139.7.6188.
72. Boots CE, Jungheim ES. 2015. Inflammation and human ovarian follicular dynamics. Semin Reprod Med 33(4):270–275, PMID: 26132931, https://doi.org/10.1055/s-0035-1554928.
73. Hu MW, Wang ZB, Jiang ZZ, Qi ST, Huang L, Liang QX, et al. 2014. Scaffold subunit Aalpha of PP2A is essential for female meiosis and fertility in mice. Biol Reprod 91(1):19, PMID: 24899574, https://doi.org/10.1095/biolreprod.114.120220.
74. Tang A, Shi P, Song A, Zou D, Zhou Y, Gu P, et al. 2016. PP2A regulates kinetochore-microtubule attachment during meiosis I in oocyte. Cell Cycle 15(11):1450–1461, PMID: 27096707, https://doi.org/10.1080/15384101.2016.1175256.